Progress in Particle and Nuclear Physics 95 (2017) 1–47

Contents lists available at ScienceDirect

Progress in Particle and Nuclear Physics

journal homepage: www.elsevier.com/locate/ppnp

Review

Interactions of neutrinos with matter

F. Vannucci

APC/LPNHE, Université Paris7-Diderot, France

ARTICLE INFO

Article history:
Available online 22 March 2017

Keywords:
Neutrinos
Interactions
Elementary particles

ABSTRACT

Neutrinos are elementary particles electrically neutral which belong to the family of leptons. As a consequence and in first approximation they only undergo weak processes. This gives them very special properties. They are ideal tools to study precisely the weak interactions, but there is a price to pay: neutrinos are characterized by extremely low probabilities of interactions, they easily penetrate large amount of matter without being stopped. Consequently, it is hard to perform neutrino physics measurements. In practice the difficulty is twofold: in order to accumulate enough statistics, experiments must rely on huge fluxes traversing huge detectors, the number of interactions being obviously proportional to these two factors. As a corollary, backgrounds are difficult to handle because they appear much more commonly than good events. Nevertheless, neutrino interactions have been detected from a variety of sources, both man-made and natural, from very low to very large energies.

The aim of this review is to survey our current knowledge about interaction cross sections of neutrinos with matter across all pertinent energy scales. We will see that neutrino interactions cover a large range of processes: nuclear capture, inverse beta-decay, quasi-elastic scattering, resonant pion production, deep inelastic scattering and ultra-high energy interactions.

All the gathered information will be used to study weak properties of matter but it will also allow to explore the properties of the neutrinos themselves. In particular, the known three different flavors of neutrinos have different behaviors inside matter and this will be relevant to give some precious understanding about their intrinsic parameters in particular their masses and mixings.

As a second order process, neutrinos can undergo electromagnetic interactions. This will also be discussed. Although the corresponding phenomena are not yet experimentally proven by actual measurements, the theory is able to calculate them and it is useful to discuss the topic since it may become an important issue to test ideas of cosmological relevance.

This review will mainly adopt an experimental point of view. Strong emphasis will be placed on important detectors which have illustrated the challenging progresses in neutrino physics; they will be described and their results confronted to theoretical predictions.

Contents

E-mail address: vannucci@in2p3.fr.

http://dx.doi.org/10.1016/j.ppnp.2017.03.003
0146-6410/

1. Introduction

There is a sacred rule in physics: energy is strictly conserved in all existing processes. In the early days of nuclear physics a very puzzling problem arose: radioactive beta-decays of natural elements seem to violate energy conservation. In December 1930, Wolfgang Pauli wrote a famous letter to his "*Radioactive ladies and gentlemen*" offering a "*desperate*" solution to this problem: he proposed the idea that a new invisible particle was emitted together with the electron detected in the observed process. He imagined the existence of a new neutral elementary object having no interactions, in practice undetectable, which carried away a fraction of the total energy available in the decay.

At that time, physicists constructed all known matter with only three objects: the proton, the neutron (not yet discovered) and the electron. Atomic nuclei were understood as assemblies of a variable number of protons and neutrons bound together with electrons orbiting around them. This is the planetary model of the atoms. This gave a very satisfactory building scheme, so that the necessity of a fourth object had to be well-motivated. Inventing a new particle was a bold act; to-day, it has become

Table 1
Table of the elementary constituents of matter.

Charge 0	ν_e	ν_μ	ν_τ
Charge -1	e	μ	τ
Charge $+2/3$	u	c	t
Charge $-1/3$	d	s	b

more common-place. But the idea was rapidly adopted by the community and, as soon as 1933, Enrico Fermi could write down the theory implementing this new particle. He invented a new interaction called the Fermi interaction, later known as weak interaction. This completed the list of all interactions existing among particles: gravitation (always negligible in this context), electromagnetic, strong (to maintain protons and neutrons bound inside the nuclei, or rather quarks tied together) and weak. Fermi also gave the name "*neutrino*", written with the greek sign ν, to this new object, since it means small neutral in Italian. In his original proposal Pauli had used the name neutron, the neutron known to-day not being discovered until 1932.

Since these historical times, the number of elementary particles has exploded to reach several hundreds but the number of interactions did not evolve. On the contrary, weak and electromagnetic interactions were recently merged into the electroweak force and nowadays theorists strive to unify strong and electroweak interactions into a single force.

Fortunately, the neutrino is not completely undetectable as suggested by Pauli, but it took a full quarter of a century to prove the existence of this new object. This shows the difficulty of experimental neutrino physics. The discovery was done at a powerful source of neutrinos, the nuclear reactor of Savannah River in South Carolina. Reines and Cowan [1] are credited for it. The result consisted in counting about 3 events per hour, when the reactor was on, in excess of what was measured during the reactor off periods. The detector built for the occasion consisted of a target of about 500 kg of doped water. It took again a long time for the discovery to be recognized by the Nobel Committee, the Prize was finally given to Reines in 1995.

2. Phenomenology of neutrino interactions

The known reactions of neutrinos with matter fall within the purview of the Standard Model (SM) of particle physics with the complication that neutrinos can no longer be considered as massless particles as assumed in the original minimal Model.

2.1. The three neutrinos and the leptonic charges

The neutrino emitted together with an electron in beta-decays produces an electron when it interacts with matter. There is a strong relationship between this neutrino and the electron. Notice that the same kind of neutrino is produced inside the Sun and also in nuclear reactors (in fact the antineutrino type in this latter case).

In the years 1960 a new problem of missing energy arose. When a π meson, abundantly found in cosmic rays, decays it emits a visible μ together with missing energy, presumably a neutrino. Is this neutrino of the same type as the one emitted in beta-decays? The answer was not obvious; it necessitated an experiment to decide. This was done at the Brookhaven Laboratory in 1964 [2]. For the first time a neutrino beam was constructed from accelerated protons, the neutrinos being of the same type as the ones originating from cosmic π decays. The detector exposed to the beam was able to finally register 29 interactions showing a clear muon track and none with an electron. This was the proof that neutrinos produced together with a muon produce a muon when they interact. The neutrinos emitted in π decays are different from the ones appearing in beta-decays. They are given different names: electron neutrino, ν_e, for the first type and muon neutrino, ν_μ, for the second. This second neutrino discovery was celebrated by the Nobel Prize before the first neutrino, as soon as 1988.

These observations are formalized by the introduction of new conserved charges (or numbers): a first leptonic charge, L_e is associated with the electron and a second one L_μ with the muon.

In 1975 at the SPEAR e^+e^- collider of SLAC a third much heavier charged lepton was discovered, the so-called tau lepton τ, and this necessitated the introduction of a third associated neutrino, the tau neutrino ν_τ [3]. Thus, three different leptonic numbers are necessary to understand the phenomenology of neutrino interactions, each of them separately conserved.

How many types of neutrinos exist in Nature? The total number of active neutrinos was precisely measured at the LEP e^+e^- collider of CERN in 1989. The result is unambiguous: there exist 3 and only 3 active neutrinos: ν_e, ν_μ and ν_τ [4].

Table 1 shows the complete list of elementary constituents which form all the ordinary matter. It is composed of 3 neutrinos of electric charge 0, 3 charged leptons of charge -1, 3 up-quarks of charge $+2/3$ and 3 down-quarks of charge $-1/3$.

2.2. Neutrinos and antineutrinos

The conservation of the three individual leptonic charges implies the existence of three different antineutrinos $\bar{\nu_e}$, $\bar{\nu_\mu}$, $\bar{\nu_\tau}$ in order to balance the various charges in all existing processes.

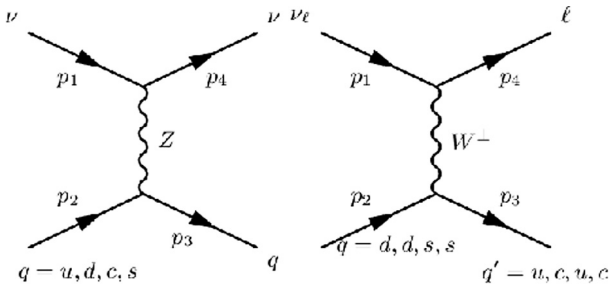

Fig. 1. Feynman diagrams showing NC (left) and CC (right) interactions of the ν_l.

Let us call L_e the first leptonic charge. ν_e and e^- will be characterized by $L_e = +1$, $\bar{\nu_e}$ and e^+ will have $L_e = -1$, and all other particles will have $L_e = 0$. In the same way, $L_\mu = +1$ for ν_μ and μ^-, $L_\mu = -1$ for $\bar{\nu_\mu}$ and μ^+ and $L_\mu = 0$ for all other particles. The same rule applies for L_τ associated to the τ and ν_τ. Each of these charges is separately conserved. We will see later that this assumption has to be mitigated because of the discovery of oscillations between neutrino flavors. As a consequence there is a total conserved leptonic charge: the number of leptons in the Universe is globally constant.

Although neutrinos are neutral particles, antineutrinos are different from neutrinos because they carry opposite leptonic charges. This explains that when it interacts a $\bar{\nu_e}$ produces a e^+. This also explains the decay of the μ^- where two different leptonic charges have to be balanced:

$$\mu^- \longrightarrow e^- + \nu_\mu + \bar{\nu_e}.$$

Beta-decays correspond to the process: n $\longrightarrow$ p$+e^-+\bar{\nu_e}$ and inverse beta-decays to the conjugate process: p $\longrightarrow$ n$+e^+ + \nu_e$.

The difference between a neutrino and an antineutrino is now clear, and experimentally a neutrino will give its charged lepton companion, and the antineutrino the associated antilepton. The result can be generalized at the level of elementary constituents, and each fermion is accompanied by a partner of opposite charge, either electric or leptonic. As a consequence, Table 1 has to be doubled to take into account the existence of the anticonstituents which have the same properties as the constituents but opposite charges, be it electromagnetic or weak. The antiquark $\bar{u}$ will have an electric charge $-2/3$.

2.3. The neutral currents

We have just discussed interactions in which a neutrino (or antineutrino) converts itself into its charged lepton companion to balance the associated leptonic charge. At accelerators, where neutrinos are predominantly of the second type, the ν_μ type, this gives the reaction:

$\nu_\mu + \mathrm{N} \longrightarrow \mu^- +$ hadrons.

But there is another possibility of interaction, which also conserves the leptonic charge. It operates when a neutrino remains itself in the final state. This corresponds to the so-called "neutral current" interaction (NC) which gives the reaction:

$\nu_\mu + \mathrm{N} \longrightarrow \nu_\mu +$ hadrons.

In 1973 the Gargamelle bubble chamber found evidence of this new type of interactions in the CERN PS neutrino beam. The interactions discussed first are called "charged currents" (CC), they exchange a $\mathrm{W}^\pm$ vector boson. On the contrary NC events are mediated by the neutral Z boson found in 1983 at the CERN proton–antiproton collider but predicted by the theory well before. In fact NC's were actively searched-for as a signature of the existence of the Z.

Schematic diagrams of the two types of interactions are shown in Fig. 1 at the level of the quarks for the hadron part.

At the time of this search, energies were relatively low ($\sim$1 GeV), and the experimental difficulty to recognize this new kind of interactions came from the fact that it is not straightforward to differentiate a NC event from a CC one producing a muon of very little energy, or an electron which is often difficult to distinguish from hadrons.

In order to understand the difficulty of the experimental problem, let us sketch the ways to detect a neutrino interaction. Obviously, neutrinos being neutral will never been seen directly and one can only detect the products resulting from their interactions. When such an interaction happens, charged particles are produced and they ionize the medium they traverse. In practice, almost all detection techniques are based on ionization, other techniques are based on Cerenkov or transition radiations.

In the old times, the apparatus of choice to study neutrino interactions was a bubble chamber which provides at the same time the target and the detector. It is a basic device which allows an unbiased way of displaying information. Interactions produced in such a device are directly shown on photographs with all their accessible details. Although it is not fast enough to accumulate the large statistics of present-day searches, bubble chambers remained for a long time an adequate apparatus, specially for neutrinos which generate a limited number of events.

A bubble chamber consisted in a container filled with a liquid which was at a temperature very close to evaporation. At accelerators, a neutrino beam arrives in bunches of short pulses lasting a few μs or ms. A moving piston released the pressure

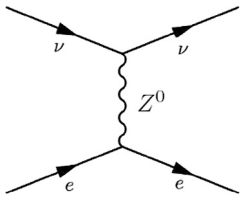

Fig. 2. Feynman diagram for $\nu_\mu + \mathrm{e} \longrightarrow \nu_\mu + \mathrm{e}$.

in the chamber at the time of the beam-crossing and bubbles started to grow in the liquid. It appeared that these bubbles grew preferentially around an electric charge, precisely where the charged particles had ionized the liquid. In practice bubbles indicated the path of the charged particles remnants of the interaction. A camera took a photograph at each beam-crossing and later the photos were scanned to search for a given topology. With this technique one can follow charged tracks with a precision of the size of a bubble, about 100 μm per point, over length which could reach meters.

Physics being an experimental science, the best theoretical speculations have to be verified by measurements before being accepted. In order to discuss interactions of neutrinos in matter, it is essential to understand the ways one has to detect them and be able to evaluate their limitations. For this reason, this review will present a selection of detectors which have illustrated the progresses in neutrino physics and, as a first example, let us describe the Gargamelle bubble chamber which discovered the NC interactions.

2.4. The Gargamelle bubble chamber

Gargamelle consisted in a large reservoir with a useful volume of 6.2 m^3 filled with a heavy liquid called freon CF_3Br in order to maximize the useful mass; it amounted to more than 9 tons. The large length of the chamber, 4.8 m, compared to the radiation length (X^0) of freon, 11 cm, ensured that electrons were unambiguously identified. A magnetic field of 2 T filled the whole sensitive volume. This allowed to measure momenta of charged particles with good accuracy through their curvature. The high performance of a bubble chamber was necessary to measure with confidence all the tracks produced in the interactions with enough precision.

The search consisted in looking for the NC process:

$\nu_\mu + \mathrm{N} \longrightarrow \nu_\mu +$ hadrons.

The Gargamelle analysis [5] had to carefully study the dynamics of the detected tracks and rely on simulations to evaluate the contribution of CC's which could mimic a neutral current. The difficulty was to ascertain the absence of any possible muon. At low energy muons are difficult to identify and neutron background is substantial. In an experimental search, a negative constraint is always more difficult to verify than a positive one. The first analysis was based on 83 000 ν pictures and 207 000 $\bar{\nu}$ pictures. The dimensions of the chamber were such that most hadrons were unambiguously identified by secondary interaction or by range-momentum and ionization. The small contamination of CC ν_e was identified by the presence of an electron track. It was crucial to check that the candidate NC events showed a spatial distribution of vertices, a hadron total energy and an angle between measured hadrons and beam direction, similar to the ones found in CC events.

After a careful evaluation of backgrounds based on a detailed Monte Carlo simulation, the analysis concluded in the observation of events without a secondary muon (or electron) at the level of:

– for neutrinos $(\mathrm{NC/CC}) = 0.21 \pm 0.03$.

– for antineutrinos $(\mathrm{NC/CC}) = 0.45 \pm 0.09$.

As can be seen, NC's are not a small correction to CC's.

A further and definite search [6] was done by observing the fully leptonic process corresponding to the clean reaction:

$\nu_\mu + \mathrm{e} \longrightarrow \nu_\mu + \mathrm{e}$.

This interaction is characterized by a single electron appearing in the final state and originating in the liquid, unaccompanied by any nuclear fragments or hadrons or γ-rays correlated to the vertex. It corresponds to the graph shown in Fig. 2.

The kinematics of the reaction is such that the electron is emitted at a small angle θ_e with respect to the known neutrino beam. The electron is expected to carry typically one-third of the incident neutrino energy which was peaked at 1–2 GeV in that search. A total of 375 000 ν and 360 000 $\bar{\nu}$ pictures were visually scanned. One event in the antineutrino film fulfilled all the prerequisites. The expected background was evaluated at 0.03 event. This was a clear signal of a NC event. In a successive analysis taking advantage of increased statistics, 3 such events confirmed the discovery. An example is given in the photograph of Fig. 3. It shows an isolated electron track directed along the direction of the neutrino beam. This discovery was a landmark to solidify the structure of the Standard Model [7]. The existence of weak NC's proved essential in this achievement.

Although bubble chambers were able to give good enough precision of measurement, they are now totally discarded. The data taking rate depended on the mechanics of the moving piston. This limited the repetition rate to at most one picture per second. Bubble chambers are too slow, and the visual analysis is very time-consuming. For a long time the technique was

Fig. 3. NC event giving a single electron as seen in the Gargamelle bubble chamber (©CERN).

sufficient since the interactions of neutrinos are rare and beam fluxes remained moderate; statistics were limited to a few 100 000 photos per measurement. In more recent years, electronic devices were developed which permitted to build fully automated detectors able to accumulate much increased statistics and, in this way, to discover much rarer phenomena.

3. Theory of neutrino interactions

In the early times, Fermi developed the "four-fermion" interaction coupling a leptonic current to a hadronic one. In this way, he could predict correctly the continuous energy spectrum for the electron emitted in beta-decays. Systematic measurements in nuclear beta-decays were found to be consistent with the V–A structure for the operators appearing in the lepton current and with a V and A structure for the nucleon current. This treatment was eventually recognized as the low-energy manifestation of a more basic interaction mediated by massive intermediate vector bosons. Later, a renormalizable theory unifying the weak and the electromagnetic interactions was formulated and found to agree with experimental data.

CC and NC describe the two types of neutrino weak interactions concerning the leptonic leg with a coupling to $W^{\pm}$ and Z^0 respectively. But the hadronic system, produced together with the lepton, can give many different topologies. In the following we will discuss various possible channels, from the low energy nuclear processes to the high energy deep inelastic scattering. Emphasis will be on important discoveries which paved the way to our present knowledge. The main experiments which have contributed to the progress in this domain will be presented with a schematic description of the corresponding detectors. This will help us in understanding the difficulties of experimental neutrino physics.

3.1. Basic elements of the standard electroweak theory

Before describing the rich variety of interaction channels, let us sketch the electroweak theory which subtends this domain of research [8].

To the lowest order, fermions are subject to the familiar QED interaction and to the residual weak interaction. They are also sensitive to the Higgs boson coupling which gives them a mass. The minimal gauge group of the electroweak theory is SU(2) × U(1), SU(2) related to the weak field and U(1) to the electromagnetic one. Two coupling constants are introduced: g for SU(2) and g' for U(1).

Beta-transitions are well described by the assumption that the e–ν_e pair is created by the operator:

$$J_\mu = \frac{1}{2}\bar{\nu_e}\gamma_\mu(1+\gamma_5)e = \bar{\nu_{eL}}\gamma_\mu e_L.$$

The factor $(1+\gamma_5)$ projects on the left-helicity component, such that e_L is the left-handed electron field. The electron being massive, there is a right-handed electron field e_R. It remains a singlet under SU(2).

If it existed, a right-handed neutrino field would have vanishing SU(2) and U(1) charges and hence no gauge interaction at all. In the following, we will see that this point will have to be clarified in light of evidences for neutrino masses. In any case, only left-handed neutrinos couple to matter, the right-handed neutrino, if any, remains sterile.

The charges act as raising and lowering operators on the doublet:

$$\begin{pmatrix} \nu_{eL} \\ e_L \end{pmatrix}.$$

With three existing neutrino species the full leptonic operator becomes:

$$J_\mu = \bar{\nu}_{eL}\gamma_\mu e_L + \bar{\nu}_{\mu L}\gamma_\mu \mu_L + \bar{\nu}_{\tau L}\gamma_\mu \tau_L.$$

The muon-decay is a fully leptonic process of the CC W-exchange type. It couples two lepton currents and its effective Lagrangian takes the canonical V–A form:

$$L_{eff} = \frac{G}{\sqrt{2}}[\bar{e}\gamma_\mu(1+\gamma_5)\nu_e][\bar{\nu_\mu}\gamma_\mu(1+\gamma_5)\mu]$$

G is the Fermi constant which is related to the gauge coupling g by:

$$\frac{G}{\sqrt{(2)}} = \frac{g^2}{8(M_W)^2}.$$

M_W being the W mass. The Fermi coupling constant is not dimensionless; its value, experimentally determined with great precision from the muon lifetime, is [4]:

$$G = 1.1663910^{-5}\ \text{GeV}^{-2}.$$

Neutral-current processes are induced by Z-exchange, and in the case of ν_μ the leptonic operator becomes:

$$J_\mu = \bar{\nu}_{\mu L}\gamma_\mu(1+\gamma_5)\nu_\mu.$$

The theory introduces three independent parameters, the masses of the W and Z bosons and a weak mixing angle also called Weinberg angle θ_W. The weak angle is related to the two gauge coupling constants by:

$$g'/g = \tan(\theta_W).$$

Thus the whole electroweak field relies on four parameters M_W, M_Z, θ_W and e, where e is the absolute value of the elementary electric charge.

Imposing the masslessness of the U(1) photon implies the further relation:

$$g\sin(\theta_W) = e.$$

As will be seen, the parameter $\sin^2(\theta_W)$ which is a basic ingredient of the electroweak model can be obtained from the ratio of antineutrino versus neutrino NC cross sections off a given target. The Yukawa couplings of charged leptons are directly related to their physical masses by the formulae:

$$g_e^2/4\pi \sim G/\pi^2 m_e^2 = 6.9\ 10^{-13}$$
$$g_\mu^2/4\pi \sim 10^{-8}$$
$$g_\tau^2/4\pi \sim 10^{-6}.$$

The smallness of the Yukawa couplings with respect to the gauge couplings and their wide disparities constitute one unsatisfactory feature of the standard theory.

To complete the theoretical overview, let us say that the vacuum state is not symmetric under the gauge symmetry. When a symmetric Lagrangian does not admit a symmetric stable vacuum solution one speaks of a spontaneous breaking of the gauge symmetry. This induces the existence of a massive neutral scalar particle, in this case the Higgs boson recently discovered at the LHC collider of CERN.

The Standard Model also relies on a particle spectrum. This spectrum is composed of:

– a set of vector particles: the massless photon and the two heavy bosons messengers of the weak force, the charged $W^\pm$ and the neutral Z^0. The masses of these two last objects are related by $M_W = M_Z\cos(\theta_W)$. To go beyond the electroweak theory, there are also 8 gluons as mediators of the strong force.

– 12 fermions which are the particles composing matter, already listed in Table 1. These 12 fermions have to be doubled with their 12 antifermions. Fermions (and antifermions) are spinor particles with spin 1/2. They exist in two categories: leptons and quarks. Leptons, among which are the neutrinos, appear in three and only three families with three left-handed doublets coupling each neutrino to its charged partner, and three right-handed singlets:

$$\begin{pmatrix}\nu_{eL}\\ e_L\end{pmatrix} e_R$$
$$\begin{pmatrix}\nu_{\mu L}\\ \mu_L\end{pmatrix} \mu_R$$
$$\begin{pmatrix}\nu_{\tau L}\\ \tau_L\end{pmatrix} \tau_R.$$

– and finally one scalar particle: the Higgs boson, for the reason mentioned above.

Gravitational waves have just been discovered experimentally, and the existence of gravitons become possible as the messenger of gravitation; the theory exists and predicts a spin 2 for this hypothetical new object.

Quarks and gluons are the basic degrees of freedom of hadronic matter. They give existence to two different families of particles: hadrons which are composed of three quarks tied together (the proton corresponds to uud), and mesons which are quark–antiquark pairs (the π^+ corresponds to $u\bar{d}$).

Electroweak interactions involve quarks which have electric and weak charges. Like leptons, quarks also exist in three families, each of them having a representative of charge $+2/3$ and one of charge $-1/3$. But quarks have another degree of freedom: they exist in three different color states. Quarks of the same flavor and different color have the same weak and electric charges.

Gluons are neutral vector particles transmitting the strong interactions, they carry color. They are governed by the SU(3) gauge symmetry and commute with the full electromagnetic symmetry, U(1) included. There is a total of 8 different gluons.

Quark masses break the SU(2)xU(1) symmetry and they arise from the quark–Higgs field Yukawa couplings in the same way as lepton masses. In the Minimum Standard Model there are no right-handed neutrino fields, consequently neutrinos are massless. Experiments have shown that neutrinos are massive, thus the Minimum Standard Model has to be completed.

3.2. Neutrino–lepton cross sections

Although difficult to observe, neutrino–lepton scattering provides the opportunity to test the standard theory in a very clean situation, free from the complications of the strong interactions. In particular a very precise measurement of $\sin^2(\theta_W)$ can be obtained from $\nu_\mu e$ scattering. In these considerations, one can assume massless purely left-handed neutrinos, thus the exact conservation of lepton flavors is valid and one can restrict the calculation to the lowest order in the electroweak interaction.

The prototype case, already shown in Fig. 2, and experimentally observed by the Gargamelle bubble chamber corresponds to a pure Z-exchange:

$$\nu_\mu + e \longrightarrow \nu_\mu + e.$$

An explicit calculation gives the result:

$$\frac{d\sigma}{dy} = 2mE_\nu\rho^2\frac{G_Z(t)^2}{\pi}\left[g_L^2 + (1-y)^2 g_R^2 - \frac{my}{\omega}g_L g_R\right].$$

There are several parameters to be defined:

– m is the electron mass, E_ν the initial neutrino energy;

– the ρ parameter is introduced for generality. It is related to the weak parameters by the relation:

$$M_W = \sqrt{\rho}M_Z\cos(\theta_W).$$

Its value is $\rho = 1$ for the simple case of the Higgs doublet model;

– G_Z is related to the Fermi constant G by the relation:

$$G_Z(t) = \frac{G}{1 - t/M_Z^2}$$

where t is the Mandelstam invariant four-momentum transfer between the initial and final neutrinos:

$$t = (p - p')^2 = -2E_\nu^2(1 - \cos\theta)$$

θ being the scattering angle;

– y is the Bjorken scaling variable, known as inelasticity, and given by $y = T/E_\nu$ where T is the final electron kinetic energy: $T = [(pp') - m^2]/m$.

Two complementary parameters appear: $g_L = -\frac{1}{2} + \sin^2(\theta_W)$ and $g_R = \sin^2(\theta_W)$.

Because of the small electron mass, the final electron is emitted within a very small scattering angle in the laboratory. This is because the cross section is quite isotropic in the c.m. system and the electrons are projected by the Lorentz transformation within an angle such that:

$$\tan(\theta) \sim 2m/\sqrt{(s)}$$

$\sqrt{(s)}$ being the center-of-mass energy. Let us remind that the squared center-of-mass energy in the lepton–nucleon system is a Lorentz invariant given by:

$$s = (p_\nu + p_e)^2.$$

For completeness one can also consider the case corresponding to the interaction of ν_e:

$$\nu_e(\bar{\nu}_e) + e \longrightarrow \nu_e(\bar{\nu}_e) + e.$$

In the first reaction open to ν_μ's the only contribution comes from Z-exchange (Fig. 2). With ν_e there is the additional contribution of W-exchange. This is shown in Fig. 4.

The calculations give the following differential cross sections:

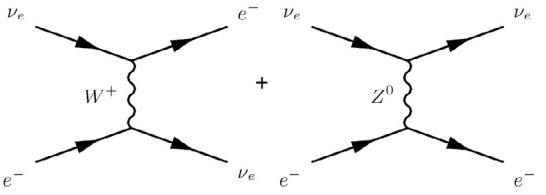

Fig. 4. Feynman diagrams showing CC and NC channels for $\nu_e + e \longrightarrow \nu_e + e$.

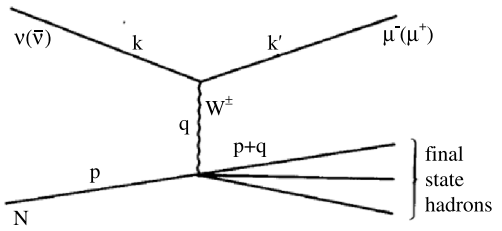

Fig. 5. Feynman diagram for neutrino–nucleon DIS.

– for $\nu_e e$

$$\frac{d\sigma}{dT} = 2m\rho^2 \frac{G^2}{\pi}[g_L^2 + (1-y)^2 g_R^2]$$

– for $\bar{\nu}_e e$

$$\frac{d\sigma}{dT} = 2m\rho^2 \frac{G^2}{\pi}[g_R^2 + (1-y)^2 g_L^2].$$

The total cross sections are respectively:

$$\sigma(\nu_e e \longrightarrow \nu_e e) = 2mE_\nu \rho^2 \frac{G^2}{\pi}[g_L^2 + g_R^2/3]$$

$$\sigma(\bar{\nu}_e e \longrightarrow \bar{\nu}_e e) = 2mE_\nu \rho^2 \frac{G^2}{\pi}[g_R^2 + g_L^2].$$

In the same way the cross sections for the other fully leptonic CC processes are:

$$\sigma(\nu_\mu e \longrightarrow \mu^- \nu_e) = 2mE_\nu \frac{G^2}{\pi}$$

$$\sigma(\bar{\nu}_e e \longrightarrow \mu^- \bar{\nu}_\mu) = 2mE_\nu \frac{G^2}{3\pi}.$$

3.3. Neutrino–hadron scattering

The cross sections for interactions on hadrons are much larger than the corresponding neutrino–electron cross section, the ratio being of the order of $M/m = 1.8\ 10^{-3}$. M is here the nucleon mass. Details of the calculations for the many possible channels can be found in [9].

The study of neutrino–hadron interactions has been of great value in understanding the structure of the fundamental interactions. In particular, the observation of NC processes has given crucial support to the standard electroweak theory and deep inelastic scattering (DIS) has confirmed the parton picture emerged from the existing electron DIS measurements.

The basic CC process on hadrons corresponds to:

$$\nu_l + nucleon \longrightarrow l^- + hadrons$$

where *l* designates one of the three charged leptons associated with the incident neutrino. Fig. 5 shows the Feynman diagram corresponding to DIS, that is the scattering at high energy transfer, practically producing a rich hadronic system. In fact, the basic process takes place on hadron constituents namely quarks and real measurements have to consider nucleon matrix elements hidden inside the so-called form-factors.

In the completely inclusive situation, only the final lepton is observed, this is often the case with accelerator neutrinos where ν_μ's produce a muon which is easily identified in a detector because of its large power of penetration. In this case, the

cross-section depends on three variables: the initial neutrino energy $w = E_\nu$, the final lepton energy w' and the scattering angle θ. The latter two variables are often replaced by the lepton momentum transfer $Q^2 = (p' - p)^2$ and the energy transmitted to the hadronic system: $\nu = w - w'$.

Alternatively, one can prefer to use the two Bjorken scaling variables:
$x = Q^2/(2M\nu)$ and $y = (w - w')/w = E_{had}/E_\nu$.
With these parameters, the inclusive differential cross-section is written as:

$$\frac{d^2\sigma}{d\cos\theta dw'} = 2ww'\frac{d^2\sigma}{dQ^2 d\nu} = \frac{1}{M}\frac{1-y}{y}\frac{d^2\sigma}{dxdy}.$$

The same results apply both to the ν_e and ν_μ cases, provided the neutrino energy is well above the muon-production threshold.

Notice that the cross section is linearly proportional to the incident neutrino energy; the higher the energy, the easier it is to produce interactions in matter. The antineutrino cross section is obtained by changing the sign of the V–A interference. In practice it is about half the corresponding neutrino cross section.

The cross sections for the NC processes are obtained by a suitable redefinition of the form-factors. In practice it is around one third of the neutrino cross section. The neutral current is flavor diagonal in the Standard Model, hence no single production of heavy quarks is expected.

3.4. The parton distribution functions of the nucleons

The study of DIS, where the only particle measured in the final state is a muon, allows to study the inner constitution of the nucleons.

The deep inelastic region will be defined by the conditions $Q^2 \gg M^2$, $\nu \gg M$, x being fixed. At high energy, neutrinos interact directly on the elementary constituents namely quarks. This allows the possibility to study the distribution of various quark species inside the nucleons.

The importance of this subject is explained by the parton description of the nucleons. Following Feynman, one assumes that the proton can be described as a cloud of pointlike objects nicknamed the partons [10]. The parton distribution inside the proton is specified by a set of probability functions, $f_i(z)$, called parton densities or pdf's. Such pdf's are the probability density to find a given parton of type i carrying a fraction z of the proton longitudinal momentum. Transverse momenta of produced particles are small and the partons are treated as being collinear with the parent nucleon. Thus, neglecting masses, the four-momentum of the parton i is given by:
$(p_i)_\mu = zp_\mu$, p_μ being the nucleon value.
Similarly, one may define other parton variables:
$\nu_i = z\nu$ and $y_i = zy$
where ν and y are the nucleon values for the energy and the Bjorken y parameter.

The DIS arises from the incoherent sum of elastic scatterings of the neutrino over each parton. After the collision, the hadronic system ends up with one parton scattered away from the others. This highly excited state then evolves into one of the multihadronic final states observed in the experiment.

It is possible to express the inclusive cross-section in terms of the elementary neutrino–parton cross-sections $d\sigma_i$:

$$\frac{d^2\sigma}{d\nu dQ^2} = \sum_i f_i(x)\frac{xd\sigma_i}{\nu dQ^2}.$$

Thus the Bjorken scaling variable x is identified as the fractional parton momentum z.

The hypothesis of partons arose independently of the idea of quarks and gluons, but one can now identify the two descriptions. Gluons do not feel weak or electromagnetic interactions, thus neutrinos will only interact with the quarks present in the nucleons. There are two kinds of quarks: first the constituent quarks which give their identity to the target hadrons and second the sea-quarks which appear in pairs of quark–antiquark. Consequently, all quark flavors are potentially present in a given hadron. It is the task of experiments to verify this hypothesis.

The inclusive neutrino cross section on a parton is the one appropriate to massless point-like spin 1/2 particles and one finds:

$$\frac{d^2\sigma}{dxdy} = \frac{G^2}{\pi}2Mw\sum_i xf_i(x)[(g_L^i)^2 + (1-y)^2(g_R^i)^2].$$

The quark–parton model predicts DIS as an incoherent sum of quasi-elastic scattering on all the partons and the corresponding cross sections can be written:

$$\frac{d\sigma}{dxdy}(\nu p) = \sigma_0 2x[[d(x) + s(x)] + [\bar{u}(x) + \bar{c}(x)](1-y)^2]$$
$$\frac{d\sigma}{dxdy}(\bar{\nu} p) = \sigma_0 2x[[u(x) + c(x)](1-y)^2 + [\bar{d}(x) + \bar{s}(x)]]$$

with:

$$\sigma_0 = \frac{G^2}{\pi} M = 1.5810^{-38}\ \mathrm{cm}^2/\mathrm{GeV}.$$

The factors $d(x)$, $u(x)$... denote the pdf's corresponding to d, u... quarks present in the hit nucleon. For example $u(x)dx$ represents the number of u-quarks in the proton carrying a momentum fraction between x and $x \pm dx$. Notice that the contributions of b and t quarks are neglected.

By studying electron–proton scattering at SLAC it was found that, for Q^2 and ν not too small ($Q^2 \geq 2\ \mathrm{GeV}^2$, $\nu \geq 2$ GeV), the structure functions are scaling: they do not depend on the two variables Q^2 and ν independently but only on a dimensionless combination in form of the Bjorken scaling variable x. The physical interpretation was given by the parton model of Feynman.

Three structure functions $W_1(x)$, $W_2(x)$ and $W_3(x)$ describe the internal structure of the nucleon as seen in neutrino–nucleon scattering. The term containing W_3 is parity violating, it does not show in electron- or muon–nucleon scattering. The scaling behavior observed at high-energies, leads to three scaling structure functions: $F_1(x)$, $F_2(x)$, $F_3(x)$, such that:

$$MW_1(\nu, Q^2) = F_1(x) = 1/2 \sum_i f_i(x)[g_L^{(i)2} + g_R^{(i)2}]$$
$$\nu W_2(\nu, Q^2) = F_2(x) = \sum_i x f_i(x)[g_L^{(i)2} + g_R^{(i)2}]$$
$$\nu W_3(\nu, Q^2) = F_3(x) = \sum_i f_i(x)[g_L^{(i)2} - g_R^{(i)2}].$$

The relation $F_2(x) = 2xF_1(x)$ typical of spin 1/2 partons results directly from these definitions.

Because of the valence quark structure of the proton (uud), there exists a constrain:

$$\int_0^1 u_V(x)dx = \int_0^1 [u(x) - \bar{u}(x)]dx = 2$$
$$\int_0^1 d_V(x)dx = \int_0^1 [d(x) - \bar{d}(x)]dx = 1.$$

Putting these results together, one can derive the following relations:

$$F_2^{\nu p}(x) = 2x[d(x) + s(x) + \bar{u}(x) + \bar{c}(x)]$$
$$F_2^{\bar{\nu} p}(x) = 2x[u(x) + c(x) + \bar{d}(x) + \bar{s}(x)]$$
$$xF_3^{\nu p}(x) = 2x[d(x) + s(x) - \bar{u}(x) - \bar{c}(x)]$$
$$xF_3^{\bar{\nu} p}(x) = 2x[u(x) + c(x) - \bar{d}(x) - \bar{s}(x)].$$

For the scattering on a neutron, the structure functions can be written in terms of the proton pdf's by isospin invariance:

$$u_n(x) = d_p(x) = d(x)$$
$$d_n(x) = u_p(x) = u(x)$$
$$s_n(x) = s_p(x) = s(x)$$
$$c_n(x) = c_p(x) = c(x).$$

For isoscalar targets, with similar amounts of protons and neutrons, and neglecting heavy quarks, one finds for neutrinos and antineutrinos respectively:

$$\sigma(\nu_l \to l^-) = \frac{G^2}{\pi} M w \left[\langle x \rangle_q + \frac{1}{3} \langle x \rangle_{\bar{q}} \right]$$
$$\sigma(\bar{\nu}_l \to l^+) = \frac{G^2}{\pi} M w \left[\frac{1}{3} \langle x \rangle_q + \langle x \rangle_{\bar{q}} \right]$$

where $\langle x \rangle_q$ and $\langle x \rangle_{\bar{q}}$ are the fractional momentum carried by all the quarks and all the antiquarks respectively. Thus, on an isoscalar target, assuming $s = \bar{s}$ and $c = \bar{c}$, one finds:

$$F_2^{\nu N}(x) = x[q(x) + \bar{q}(x)]$$
$$xF_3^{\nu N}(x) = x[q(x) - \bar{q}(x) + 2(s(x) - c(x))]$$
$$xF_3^{\bar{\nu} N}(x) = x[q(x) - \bar{q}(x) - 2(s(x) - c(x))]$$

with $q = u + d + s + c$ and $\bar{q} = \bar{u} + \bar{d} + \bar{s} + \bar{c}$.

One sees that neutrinos and antineutrinos probe different components of the nucleons and one can extract information on the internal structure of the target by comparing the results with different beams.

This demonstrates that the structure function F_2 measures the density distribution of all quarks and antiquarks within the proton, while F_3 averaged over ν and $\bar{\nu}$ measures the valence-quark distribution.

We will see that experiments verify in first approximation these predictions and the various flavor contributions which can be extracted give a clear picture of the internal structure of the nucleons:

$\langle x \rangle_q + \langle x \rangle_{\bar{q}} \sim 0.50$ and $\langle x \rangle_{\bar{q}} \sim 0.07$.

Consequently, this verifies the vision of nucleons containing valence or constituent quarks carrying about 1/3 of the nucleon momentum, together with sea quarks carrying an extra 1/6. But quarks and antiquarks do not exhaust the total nucleon momentum, the missing part representing about 0.50 has to be carried by the gluons which are not probed by neutrinos.

3.5. The high energy limit

In the high energy limit, the differential cross section is dominated by the form-factors of the hit nucleon. The electromagnetic form-factors are known from electron scattering. They have been found to show approximately a dipole behavior:

$$\frac{g_E(t)}{g_E(0)} \sim \frac{g_M(t)}{g_M(0)} \sim \frac{1}{(1 - t/m_V^2)^2}$$

with the so-called vector mass being $m_V \sim 0.85$ GeV/c^2.

The axial form-factor $g_A(t)$ can be determined by using the elastic neutrino–nucleon scattering. It will be parameterized likewise and one introduces an axial mass m_A. Experimentally, it will be obtained by evaluating the difference between neutrino and antineutrino cross sections and the numerical result obtained for m_A is very similar to m_V.

Owing to the rapid fall-off of the form-factors at large t, the elastic cross section approaches a constant limit at high energies. The form-factors cut the differential cross section for values of $t \geq m_{V,A}^2$, and one obtains: $\sigma \sim 10^{-38}$ cm^2.

This is extremely small compared to electromagnetic cross sections which can reach 10^{-27} cm^2.

4. Low energy neutrino interactions

Neutrino–hadron interactions have been observed over a wide energy range, from 200 keV for solar neutrinos up to energies of several 100 GeV in the case of accelerator neutrinos. Notice that recent indications obtained by the IceCube telescope set-up in the ice of the South Pole give evidence for astrophysics neutrinos of extra-galactic origin carrying energies in excess of PeV (10^{15} eV).

Interaction processes go from neutrino–nucleon elastic scattering to DIS producing a complicated hadronic system. The various channels explored by experiments will be reviewed. In all cases, the weak current keeps the generic V–A form.

We will first describe some low energy phenomena. Low energies are typically the ones characterizing neutrinos produced by radioactive sources, the Sun and nuclear reactors. The range is limited to ∼10 MeV. Various possible channels have been investigated, and we will list them in the order of historical importance. In this regime the effect of massive vector bosons disappear from the theory.

4.1. The discovery channel

A first reaction one can think of is the neutrino capture on radioactive nuclei:

$$\nu_e + A_N^Z \longrightarrow e^- + A_{N-1}^{Z+1}.$$

This reaction is unique because the process is exothermic and hence no energy is required to initiate it. It could be a possible channel to detect cosmological neutrinos which represent the Holy Grail of this domain of physics but the cross sections are desperately low. A variant of it will be used for the detection of solar neutrinos which are of the ν_e type at production.

The experiment discovering the existence of the particle hypothesized by Pauli was done taking advantage of neutrinos emitted by a nuclear reactor. Neutrinos produced in a nuclear reactor are of the $\bar{\nu}_e$ type, they come from beta-decays of fission products of the reactor fuel like ^{235}U, ^{239}Pu, ^{241}Pu and ^{238}U. There are many secondary products and each decay channel goes to several excited levels of the final nucleus. The energy spectrum is the sum of many individual beta emissions. The final spectrum peaks below 2 MeV and extends up to 10 MeV, and the total flux reaches the enormous value of $10^{21}\bar{\nu}_e$/s in the case of a commercial reactor.

The original detection was done with an apparatus exposing a sensitive target made of liquid scintillator in such a high flux. The interaction channel of choice is similar to the one responsible for ordinary beta-decays except that the neutrino is interacting with the target nucleus:

$$\bar{\nu}_e + A_N^Z \longrightarrow e^+ + A_{N+1}^{Z-1}.$$

At the level of nucleons this can be thought of as the CC inverse beta-decay of the proton:

$$\bar{\nu}_e + p \longrightarrow e^+ + n.$$

This reaction is no more exothermic, the threshold energy on protons is 1.8 MeV. This is the preferred channel used to detect reactor neutrinos. In the original Savannah River experiment, a total volume of 1400 liters of organic liquid scintillator doped with an admixture of cadmium octoate was exposed to the $\bar{\nu}_e$ flux delivering 1.3 $10^{13}/\mathrm{cm}^2/\mathrm{s}$. The produced positron was detected by a first pulse of light emitted immediately at the time of the interaction, while the accompanying neutron was moderated by the protons in the scintillator and then captured in cadmium. A delayed signal came from gamma rays created as a consequence of the capture process. Thus the signature required the coincidence of two pulses separated by a known time interval.

At the origin of almost all detection process there is the phenomenon of ionization produced by charged particles while they traverse a sensitive medium. That was already the case in bubble chambers where ionization triggered the formation of bubbles. Ionization is an atomic phenomenon which liberates electrons on the passage of an energetic charged particle. These electrons can go back to the atoms if there is no outside perturbating force, light is produced during this phase and this light can be detected at some distance if the medium is transparent. Liquid scintillators offer a very effective medium to implement the process because of the high conversion factor between the initial ionization and the final emitted light. The produced light can be efficiently detected by photomultiplier tubes disposed on the periphery of the sensitive volume. The set-up is very fast, it reacts at the 1 ns level and because of the large number of photons produced in the process the energy resolution is quite good.

The produced e^+ stops in the detector volume within a few cm after its creation, releasing all its energy in a succession of bremsstrahlung then e^+e^- pair creation from photon materialization. Light is detected almost immediately. With this technique, the amount of emitted light is proportional to the energy of the shower, namely the energy of the positron. In parallel, the produced neutron slows down then is captured at rest producing several photons of MeV energies. These photons deposit all their energy in the liquid first giving e^+e^- pairs, then an electromagnetic shower. This second light pulse arrives some time later. The coincidence of these two consecutive pulses reduces the background to a minimum and gives a very reliable signature of the searched-for interaction with information on deposited energies and time-structure.

The detection reaction just discussed is very well adapted to neutrino energies of a few MeV as are those produced at reactor plants. It was efficiently used, not only in the pioneer discovery experiment, but by a long series of experiments. In the years 1980 the ILL-Grenoble [11], Goesgen [12], Bugey [13] and Krasnoyarsk [14] experiments were set-up, followed in the years 1990 by Chooz [15] and Palo Verde [16], Kamland [17] in 2000 and more recently by Double Chooz [18], Reno [19] and Daya Bay [20] experiments. A much bigger set-up is in preparation called JUNO [21] which will be situated 50 km away from powerful nuclear plants in China.

The knowledge of the neutrino flux produced in a reactor has large uncertainties. Recently, results of old experiments have been revisited with new calculations of the spectrum incorporating a more comprehensive model of the fission production [22]. The new treatment has the effect that it systematically raises the expected flux from reactors providing some tension between the data and the theoretical predictions. This observation could be interpreted as a sign of the production of sterile neutrinos. New measurements are being prepared.

4.2. The Chooz experiment

As an example of an experiment using the technique discussed above, let us describe the Chooz detector which took data near the Chooz reactor situated at the border between France and Belgium.

A commercial reactor (4 GW power) produces a lot of $\bar{\nu}_e$, on the order of $10^{21}/\mathrm{s}$. The detector was positioned 1 km from the source since it aimed at measuring oscillations. The target consisted in 5 tons of liquid scintillator loaded with gadolinium, contained in a transparent sphere of acrylic fabric seen by 120 photomultiplier tubes.

This sensitive mass corresponds to about 10 times the size of the Savannah River pioneer experiment. Gadolinium was chosen, instead of cadmium, because it is very effective for neutron capture. It has a huge neutron capture cross section of 50 000 barns and releases in average 3 γ-rays carrying a total of 8 MeV, well above backgrounds from local radioactivity, after a capture time of typically $\sim$30 μs.

The target was surrounded by a second much bigger vessel full of 120 tons of liquid scintillator serving as gamma catcher, buffer and inner veto. This shields very effectively against external background coming from fast neutrons, stopping muons or energetic photons entering from the outside. Also an outer muon veto was installed on top of the detector against cosmic rays. By relative timing between the photomultiplier tubes hit, it was possible to reconstruct the interaction point within 20 cm. The energy resolution reached 6 10^{-2} at 8 MeV, and the energy threshold was as low as 1 MeV. The trigger consisted in two pulses correlated in space and delayed by $\sim$ 30 μs. The experiment detected about 30 events/day.

4.3. The radiochemical method

Neutrino interactions on nuclear isotopes have been studied in detail in the case of ^{12}C. This offers a clean test for theory and experiment. For example the exclusive reaction $^{12}\mathrm{C}(\nu_e, e^-)^{12}\mathrm{N}$ has been measured by KARMEN [23] and LSND [24]. The reaction $^{12}\mathrm{C}(\nu_\mu, \mu^-)^{12}\mathrm{N}$ was also measured by the LSND collaboration [25]. But the interactions of neutrinos on nuclei are mainly illustrated by experiments trying to measure the solar neutrino flux.

The energies of solar neutrinos are, for the most part, lower than the ones obtained at nuclear reactors. The full spectrum is shown in Fig. 6 with its different components produced through different production chains. The first and main one, the so-called pp-chain, stops at 430 keV.

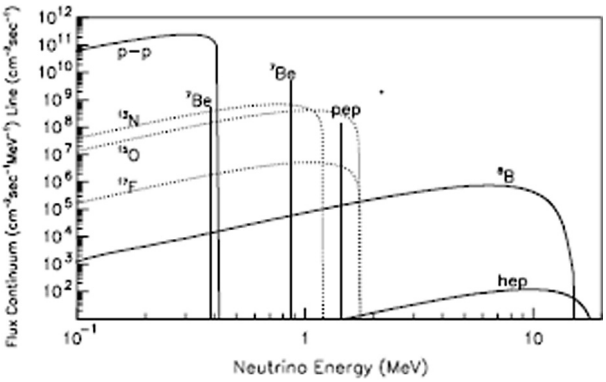

Fig. 6. The flux of solar neutrinos.

The detection of reactor neutrinos was done using electronic devices; solar neutrinos first observations used very different techniques. Historically, the first attempt to detect them started in the years 1970, it was done using a radiochemical method. Ray Davis and collaborators [26] constructed a large tank filled with 600 tons of a liquid containing chlorine (C_2Cl_6 tetrachloethylene) built in the Homestake mine in South Dakota. He received the Nobel Prize for his result in 2002.

The detection process used here was the absorption on chlorine:

$$\nu_e + {}^{37}\mathrm{Cl} \longrightarrow e^- + {}^{37}\mathrm{Ar}.$$

The threshold for this reaction is 814 keV, making the experiment sensitive to two important components of the total solar flux: the ν_{Be} which gives a monoenergetic peak at 860 keV and the high energy tail of ν_B. The produced ^{37}Ar atoms are radioactive with a half-lifetime of 37 days, and the idea was to recover these atoms and count them by characterizing their radioactive signature through their electronic decay. The rate estimate was based on solar models existing at the time which predicted about one atom produced every day; that fixed the design size of the tank to 600 tons. The analysis required a complicated chemical analysis. The whole volume of liquid was recirculated every week, hoping to extract a few candidate atoms. The argon was then separated, using a flow of helium bubbled through the tank and it was trapped in a small proportional counter where electron-capture decays of the ^{37}Ar were detected via their Auger electron emission.

Unfortunately (or fortunately!) the result remained ambiguous for a long time. It was not in agreement with the theoretical prediction based on the well-known solar luminosity. The experiment accumulated data over a period of 30 years, obtaining a fraction of the expected statistics. At the end of this very long data taking period, the average extraction rate amounted to the equivalent of about 1/3 of a radioactive atom per day, 3 times less than anticipated. At that time the conclusion was not clear at all.

Long after the pioneer search by Ray Davis and collaborators, the same method was used with gallium atoms as active target. The cross-section is higher, necessitating a less voluminous target, in practice limited to 30 tons of gallium. Two experiments were set-up, one in Europe named Gallex [27] assembled under the tunnel of the Gran Sasso laboratory in Italy and one in Russia named Sage [28]. Both targets contained gallium in the form of a liquid: 100 tons of $GaCl_3$ for Gallex, 60 tons of gallium metal (which is liquid) for Sage.

The reaction on gallium is:

$$\nu_e + {}^{71}\mathrm{Ga} \longrightarrow e^- + {}^{71}\mathrm{Ge}.$$

The threshold for this reaction is now much lower than in the case of ^{37}Cl, 233 keV, making this experiment the first sensitive to all sources of solar neutrinos in particular the dominant low energy pp chain. Again the produced atom ^{71}Ge is radioactive with a half-lifetime of 11 days.

The result was published in 1992. It confirmed the deficit seen by Ray Davis: only 0.60 of the predicted flux was detected. The gallium experiments had a great advantage, it was possible to calibrate the extraction process by exposing the target to a well-known very intense (MCi) radioactive source of ^{51}Cr [29]. This test gave a satisfactory result, experimental measurements were in agreement with the predictions, although the values were found slightly lower than anticipated. This allowed a direct measurement of the extraction efficiency and validated the method.

After this series of measurements, the deficit of solar neutrinos was accepted by the community.

4.4. The elastic scattering on electrons

In the flux of solar neutrinos, there is a much higher energy component coming from the ^{9}B channel and extending up to 15 MeV. Although the corresponding flux is 10^{-4} of the total one, this gives a new possibility to search for these neutrinos, but a very large experiment is required since the flux is tiny and the cross section of the chosen channel very much reduced.

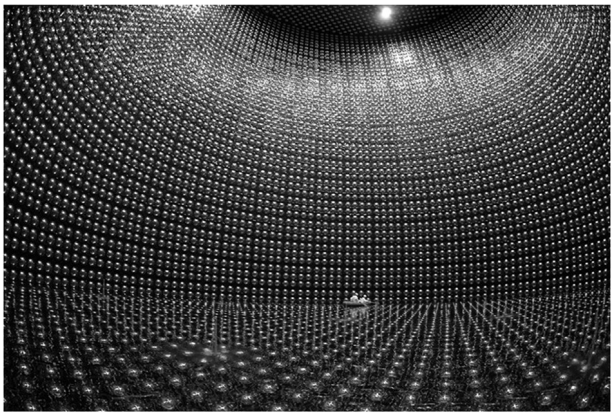

Fig. 7. Photograph of the SuperKamiokande detector.

The idea was to detect solar neutrinos by elastic scattering on electrons. As was discussed, this channel is theoretically clean and is experimentally important because it allows to measure the arrival direction of the neutrinos. The two-body scattering is governed by the dynamics of the process and the phase space available in the interaction. As a consequence the electrons are produced in the forward direction, they keep the direction of the incident neutrino. It is the favored way adopted by the very large water Cerenkov detectors to measure solar neutrinos. But the cross-section is very small, only $\sim$1/2000 of the cross-section on nucleons.

The technique is the following: the incoming neutrino exchanges energy with an atomic electron of the water molecule. Since the energy of solar neutrinos extends up to 15 MeV, the ejected electron can have enough energy to release Cerenkov light along its path before it stops. In fact the detection threshold was set in order to reduce to a manageable level the surrounding backgrounds. It was originally chosen around 7 MeV and gradually lowered when the conditions improved. It is now at 3.5 MeV. The electron track can cross several centimeters of water and this gives enough light to be detected by photomultiplier tubes which surround the sensitive volume.

The method was originally used by two detectors Kamiokande [30] in Japan and IMB (Irvine–Michigan–Brookhaven) [31] in Ohio State. Originally, these detectors were designed to search for proton decays. They had the fantastic chance of detecting a burst of neutrinos coming from the supernova explosion SN1987A. They consisted in a large cylindrical tank filled with 2 ktons (1 kton fiducial) of purified water. The initial threshold of 7 MeV made the experiments sensitive only to a fraction of the high energy tail of the ν_B mode. But this was low enough to distinguish the neutrinos from background because the momenta of the recoil electrons are strongly correlated with the direction of the Sun. It clearly showed for the first time that neutrinos are emitted by the Sun confirming the nuclear origin of solar energy.

4.5. The SuperKamiokande experiment

The archetypal detector using this method is the, still active, SuperKamiokande [32] experiment. A photograph of the container during its water filling is shown in Fig. 7.

It consists of a huge cylindrical reservoir of 50 ktons (40 m high by 40 m in diameter) of purified water, amounting to 22 ktons of fiducial mass, the exterior envelope of the full volume being used to reject background coming from the surrounding rock. It is situated in a mine under a Japanese mountain in order to be shielded against the always dangerous continuous flux of cosmic rays. Neutrino interactions are rare, it is necessary to protect as well as possible the detector against the much more abundant flux of muons falling from the atmosphere.

The Cerenkov light is produced in a cone along the track of the ejected electron. It is detected by large photomultiplier tubes which cover a large fraction of the exterior walls of the reservoir. A total of 11 000 tubes having 40-cm in diameter cover more than half of the total wall surface.

The detection threshold was gradually lowered to 3.5 MeV. SuperKamiokande coud detect and measure about 15 interactions per day having the prescribed signature, out of a flux of billions of billions of solar neutrinos traversing the volume. Because of the kinematics of the reaction, it is possible to reconstruct within a few degrees in real time the position of the Sun in the sky. The result detected about 0.40 of the expected flux, this was enough to clearly confirm the deficit seen by radiochemical measurements.

This deficit of solar neutrinos remained a mystery for a long time. With measurements becoming more precise, it was taken as a proof of the very special phenomenon of oscillations, the spontaneous change of solar ν_e into other flavors of neutrinos during the trip from their production point in the center of the Sun to their detection point on Earth.

4.6. The ultimate discovery channel

The deficit of solar neutrinos was proven before the year 2000, with several experiments using different techniques all measuring a flux substantially smaller than the predicted one, and this deficit seemed to vary with energy. It suggested oscillations but the solution to this problem was not unique. Different sets of parameters could explain the existing measurements. A final confirming experiment was necessary. This came with the Canadian Sudbury Neutrino Observatory (SNO) [33], located 2100 m underground in the Creighton Mine in Sudbury, Ontario.

The technique is very similar to the one used by SuperKamiokande: a large reservoir (1 kton) of a transparent liquid is spied by a large number of light sensors (∼9600), but the target was made of heavy water instead of normal water. In fact, it used the Canadian strategic reserve in this expensive material, necessary as moderator for the functioning of the nuclear reactor plants of the country. The book value of the precious liquid stood at 300 millions dollars, but it was given on loan for a symbolical 1 dollar.

Heavy water D_2O contains deuterons which bind a proton and a neutron in the nucleus instead of a single proton. Direct cross section measurements on deuterium targets were carried out in the past using antineutrinos from nuclear reactors at Savannah River [34] or Bugey [35]. The measurements were in agreement with calculations within $\pm 20\ 10^{-2}$, and the technique seemed well adapted to definitely solve the solar neutrino puzzle.

The difference of target structure is crucial: deuterium has a very small binding energy of 2.2 MeV, and a neutrino interacting with the deuteron can easily break the nucleus. While the elastic scattering on electrons used in SuperKamiokande is essentially due to the ν_e, this new NC process is equally open to all three neutrino flavors. This allows the first integrated measurement of the total neutrino flux received from the Sun, independently of their flavor.

In practice, SNO can measure three different and complementary interaction channels:

– CC's producing an electron, this is only possible with ν_e and the mode opens up above an energy threshold of 1.4 MeV:

$$\nu_e + d \rightarrow p + p + e^-.$$

An isotropic electron shower tags this type of reaction and the electron energy is measured by the amount of produced light.

– elastic scattering on electrons like in SuperKamiokande, ν_μ and ν_τ can contribute but their cross-section is only 1/6 of that of ν_e because of W-exchange in this latter case:

$$\nu_e + e^- \rightarrow \nu_e + e^-.$$

Here the direction of the signal with respect to the position of the Sun is used to select the candidate events.

– NC's breaking of the deuteron. A neutrino dissociates the deuteron, breaking it into its individual constituents neutron and proton. The neutrino continues on with slightly less energy, and all three neutrino flavors are equally likely to participate in this interaction. The channel opens up as soon as the neutrino energy is above 2.2 MeV:

$$\nu + d \rightarrow p + n + \nu.$$

In this last case, the signal comes from characteristic gamma-rays emitted after the neutron capture. To detect this occurrence, two techniques were used. During a first period 2 tons of salt were added into the water. A second period profitted of the installation of proportional tubes filled with ^{3}He inserted inside the target. These tubes were efficient neutron counters.

In summary, SNO was able to measure separately the flux of ν_e and the total flux of all types of neutrinos coming from the Sun. It proved without ambiguity that the total detected flux is in agreement with the theoretical prediction, but ν_e constitute about 1/3 of the flux when arriving on Earth, the rest has oscillated to other neutrino flavors [36]. The long-standing puzzle of the solar neutrino deficit was definitely resolved and the result was recognized by the Nobel committee in 2015.

In parallel, the Borexino detector set under the Gran Sasso mountain gave the first direct observation of pp neutrinos and measured precisely the ^{7}Be neutrinos. Borexino is based on 300 tons of extremely low radioactivity liquid scintillator.

5. High energy neutrino interactions

At accelerators, neutrino beams allow to study interactions of much higher energies. They are predominantly of the ν_μ type with a small contribution of ν_e at the $\sim 10^{-2}$ level. The study of neutrino–hadron interactions has been of great value in understanding fundamental interactions but has also given essential information on the structure of the hadrons.

When moving up in energy, the description of neutrino scattering becomes increasingly more diverse and complicated. We will be concerned with several categories:

– elastic and quasi-elastic scattering. Neutrinos can elastically scatter off an entire nucleon liberating a nucleon or multiple nucleons from the target. In CC interactions this gives the quasi-elastic (QE) channel whereas for NC events it is referred to as elastic scattering.

– at intermediate energies, below $\leq$5 GeV, neutrinos can excite the target nucleon to a resonance state which then decays to a variety of mesonic final states. This energy regime produces a variety of final states. It is often referred to as the transition region because it corresponds to the boundary between QE scattering in which the target is a nucleon and DIS in which the target is one of the constituent partons inside the nucleon.

– in DIS, the neutrino has enough energy to resolve the individual quarks of the nucleon. This type of interactions manifests itself in the creation of a hadronic shower. From the observational point of view, the DIS regime corresponds to large Q^2 events showing hadronic final states with more than one particle.

Most of the knowledge in the intermediate energy range comes from early experiments, often using bubble chambers, that collected relatively small data samples. Over the years, interest migrated to higher energies available since the years 1975's to yield larger event samples (the cross section increases linearly with energy) and the focus centered on measuring electroweak parameters and structure functions with DIS events.

Notice that antineutrino cross sections are typically less well-measured than their neutrino counterparts. This is due to lower statistics because antineutrinos are less abundantly produced in a beam and their interaction cross sections are half that of the neutrinos ones.

The presentation will follow the historical development that occurred with neutrino beams, and QE scattering will appear as one of the last measurements. But before starting this section, let us see how a neutrino beam is obtained.

5.1. Neutrino beams

The discovery of the second type of neutrinos made at the Brookhaven Laboratory took advantage of the first neutrino beam ever built at an accelerator. Protons accelerated to around 30 GeV were sent on a metallic target where π's and K's are produced abundantly. Then the mesons are let decay. One of the difficulties in constructing a beam is to shield the detector against all charged particles, protons which have not interacted, pions and kaons which have not decayed and above all muons produced together with the neutrinos.

As an example, the CERN SPS beam has been in operation for many years. Let us describe in some details the last phase of the West Area Neutrino Facility (WANF) used in the years 1990.

The neutrinos are predominantly produced from the decays in flight of the secondary π and K mesons originating from the 450 GeV protons impinging on a beryllium target. The SPS cycle repeats every 14.4 s. The protons were extracted from the SPS in two 4 ms long spills with up to $\sim 10^{13}$ protons in each one. The beam is thus bunched in time. This is a very important feature against background: one can use the on/off technique to subtract it. Over a few years, an experiment could collect up to several 10^{19} protons incident on the target (pot's).

The target station consisted of several beryllium rods, 3 mm in diameter, positioned longitudinally along the proton line. The secondary pions and kaons were focused by a pair of coaxial magnetic lenses, called the horn and the reflector. In such a system, charged particles were deflected by the toroidal field of the lenses between two coaxial conductors carrying equal and opposite currents so that focusing particles of one sign implied defocusing particles of the opposite sign. In order to harden the neutrino spectrum, the horn and reflector were displaced 20 m and 90 m from the target, respectively.

This set-up allows to easily switch from a neutrino to an antineutrino beam just by changing the polarity in both horn and deflector. The sections between the horn and the reflector and between the reflector and the decay tunnel were enclosed in helium tubes of 80 cm diameter for a total length of about 60 m in order to reduce the absorption of secondary particles which are the neutrino parents. Collimators reduced the contamination by intercepting the defocused secondaries.

The mesons were allowed to decay in a 290 m long vacuum tunnel. Shielding made of iron and earth followed to range out muons and absorb hadrons. A toroidal magnet, operated at 3 kA located at the entrance of the iron shielding, deflected muons which would pass outside the shielding. Finally the detectors were located $\sim$ 800 m from the target.

A neutrino beam monitoring system based on the detection of muon yields at several depths into the iron shield was built. Silicon detectors provided an absolute flux measurement. A detailed GEANT simulation of the beam line predicted the neutrino energy and radial position distributions. With such a set-up, a Monte Carlo program calculated the relative abundance of neutrino species. The result was [37]:

$$\nu_\mu{:}\bar{\nu_\mu}{:}\nu_e{:}\bar{\nu_e} = 1.00{:}0.061{:}0.0094{:}0.0024$$

with average energies of 23.5, 19.2, 37.1 and 31.3 GeV respectively. The spectra are shown in Fig. 8 with the various origins of the different flavors. The high neutrino energy increased the sensitivity of experiments to CC ν_μ interactions which have an energy threshold of 3.5 GeV. The ν_τ flux is very much suppressed at these energies, down to less than 10^{-4} of the total. Typically, the number of neutrinos produced in the solid angle of a detector positioned at $\sim$800 m is 1/1000 of the number of protons impinging on the target.

Other types of neutrino beams have been built. They represent variations on the main design just sketched:

– a beam dump type consists in a very heavy target stopping all secondary particles produced by the incoming protons. The flux is much lower but it is enriched in neutrinos coming from the decay of heavy quarks. Such a beam was used by the DONUT experiment [38] to detect a few examples of ν_τ interactions because this last flavor is essentially produced in charm decays.

– at meson factories, like LAMPF, neutrinos come from pions at rest. The interest is to produce an almost monoenergetic beam of 30 MeV ν_μ's.

– the solution of narrow-band beams will be discussed later with some details and also its modern version of f-axis beams will be presented.

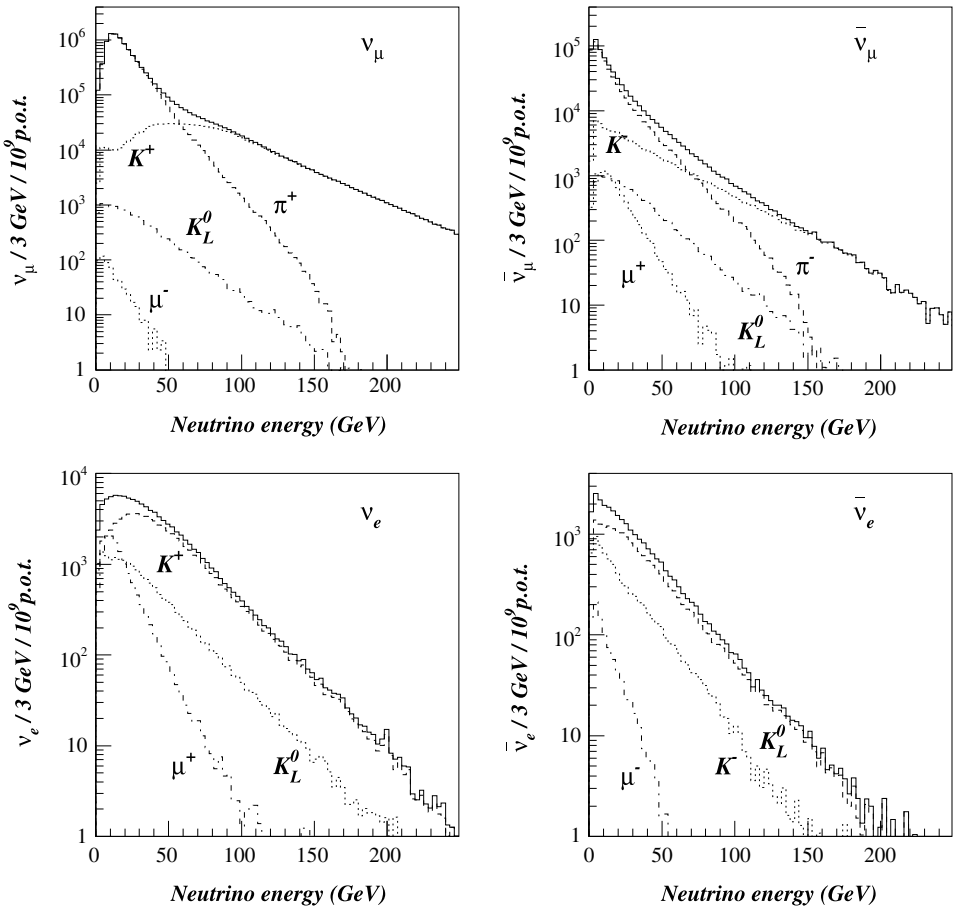

Fig. 8. Fluxes of the various neutrino species in the WANF beam at CERN.

5.2. Total cross-sections

At high energy the neutrino can begin to resolve the internal structure of the target and scatter off an individual quark inside the nucleon. The DIS process has long been used to validate the Standard Model and probe nucleon structure. Over the years, experiments have measured cross sections, x and y distributions, electroweak parameters, coupling constants, nucleon structure functions. The last point is particularly important since neutrino DIS has confirmed the parton picture of the hadrons emerged from deep inelastic electron- or muon–proton scattering and have been crucial in determining the quantum numbers of the hadron constituents which led to the determination of quantum chromodynamics (QCD) as the basic theory of the strong interactions.

We will mainly consider DIS of ν_μ and $\bar{\nu_\mu}$, in both CC and NC processes, but ν_e and $\bar{\nu_e}$ interactions have also been measured, although with less accuracy; we have seen that high energy beams obtained at accelerators produce essentially the muonic type of neutrinos.

The first measurement that can be done is the variation of the cross section as a function of the neutrino energy. This has been studied since the advent of neutrino beams. The difficulty of the measurement stems first from the fact that cross sections are small but also because a neutrino beam is far from monoenergetic.

The measurement of absolute neutrino cross sections depends on the precise monitoring of the incoming flux. A big benefit comes from the initial knowledge of the neutrino energy on an event-by-event basis. This is possible with the use of a narrow band beam where π's and K's from primary proton interactions are selected by a magnetic channel in a small momentum bite immediately after their production. The leptonic meson decay is a two-body process. By virtue of the correlation between the neutrino decay angle and its energy, the latter can be deduced from the measurement of the neutrino impact radius on a downstream detector.

High energy (up to more than 300 GeV) narrow-band beams were available at CERN and Fermilab and exploited by several detectors. The disadvantage of this kind of beam is that it gives a drastically reduced flux compared to the full wide band beam.

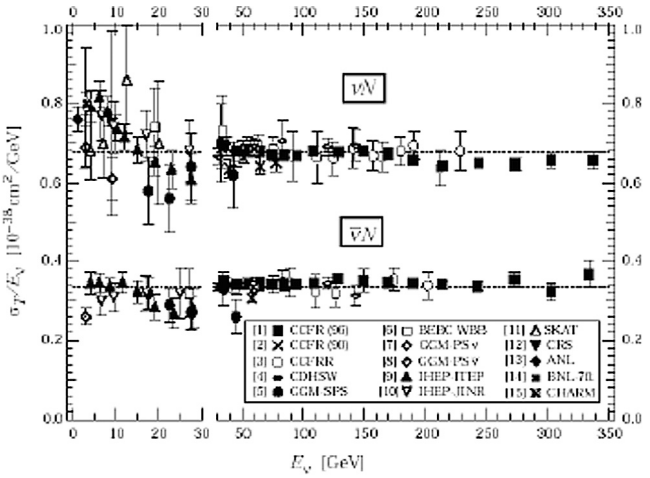

Fig. 9. Ratios of inclusive cross sections over energy as a function of energy.

Concerning the detectors, ideally they should have a mass as large as possible to accumulate high statistics and a granularity as fine as possible to permit a good precision on the measurement of the reaction products. These two demands are difficult to associate and in the history of neutrino experiments each detector privileged one or the other of these two aspects.

CC interactions are selected by the unique detection of a muon track. To isolate DIS events, experiments typically apply kinematic cuts to remove QE and resonance-mediated contributions from their data. Fig. 9 shows measurements of the inclusive CC cross sections from NuTeV [39], NOMAD [40], MINOS [41] together with older results. As can be seen the CC cross section is measured to a few percent accuracy in the region 30–350 GeV. A linear dependence on the neutrino energy is clearly exhibited, this gives a nice confirmation of the quark parton model predictions.

These results allow to extract the following inclusive cross sections:

$$\sigma(\nu N) = 0.7\ 10^{-38}\ \mathrm{E\,(GeV)\,cm^2}$$
$$\sigma(\bar{\nu} N) = 0.3\ 10^{-38}\ \mathrm{E\,(GeV)cm^2}.$$

Practically, and to give a first estimate, the number of ν_μ interactions in a target is given by the formula:

$$N = 0.7\ 10^{-38} E N_A L \rho \Phi$$

where E is the neutrino energy in GeV, ρ the density of the detector's medium, L the length of the target in cm and Φ the incident flux of neutrinos. N_A is the Avogadro number.

With these numbers one can check that only 1 solar neutrino out of 1 billion interacts when crossing the entire diameter of the Earth. On the other hand, the Earth becomes opaque for neutrinos having energies above 10^6 GeV. This type of energy is found in cosmic rays. Notice that, at much higher energy, the cross section is not proportional to energy any more, it saturates.

5.3. The CDHS experiment at CERN

We just saw that beams can produce a huge number of neutrinos. Let us turn now to one of the first large-scale generic neutrino detectors to be active at an accelerator complex. It was installed in the SPS neutrino beam at CERN. It is known as the CDHS experiment [42] and took data from 1976 until 1984. It consisted in a collaboration of CERN, Dortmund, Heidelberg and Saclay, later joined by Warsaw. The experiment provided a good measurement of muons signaling an interaction, it was optimized to study inclusive DIS of ν_μ's and $\bar{\nu_\mu}$'s in iron. At the energies involved here, muons lose about 700 MeV in penetrating 1 m of iron, thus they could be followed over several meters.

The detector had a mass of 1250 tons combining the functions of a muon spectrometer and a hadron calorimeter. It extended over a length of 20 m. It consisted of 19 magnetized hexagonal iron modules, 3.75 m in diameter. Iron served at the same time as target for the neutrinos, absorber for the hadrons and analyzer for the muons. Hexagonal multiwire proportional chambers detected the charged tracks between modules. Each module was composed of a sandwich of 2.5 cm thick iron slices together with scintillator planes for the active part of the calorimeter. Thus the granularity was 2.5 cm of iron, that is about 1.4 X^0. The iron slabs were magnetized with a magnetic field reaching the saturation value in iron of about 1.6 T.

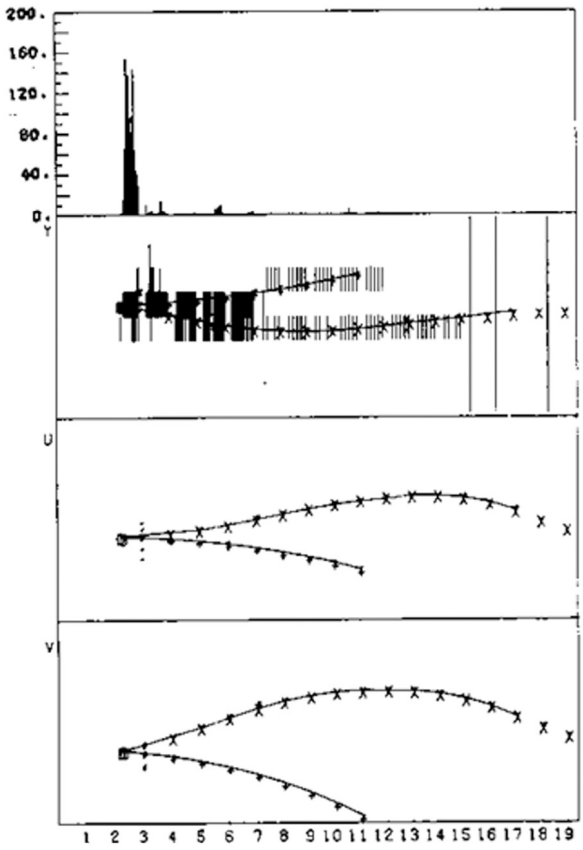

Fig. 10. A ν_μ interaction with 2 muons as seen in the CDHS detector(©CERN).

The main interactions to be studied were CC's:

$$\nu_\mu + \text{Fe} \longrightarrow \mu^- + \text{anything}$$

and NC's:

$$\nu_\mu + \text{Fe} \longrightarrow \nu_\mu + \text{anything}.$$

Due to their power of penetration, muons could be identified as long tracks reconstructed in the iron. Because of the magnetization, tracks were curved and the curvature measured their energy. Fig. 10 shows an example of an event with two muons and some activity around the vertex.

The muon reconstruction resulted in a momentum resolution:

$$\delta p/p = 0.20/\sqrt{L(m)}.$$

The rest of the particles produced in the interaction were rapidly absorbed giving rise to short showers which deposited energy in the scintillator slabs. The corresponding resolution on electromagnetic showers was limited to:

$$\delta E/E = 0.30/\sqrt{E(\text{GeV})}.$$

5.4. The CHARM experiment at CERN

The CHARM detector [43] took data in the same beam line as CDHS. In fact it was built in the same experimental hall just behind CDHS. Compared to its companion, CHARM was characterized by a finer granularity. The detector had two parts, the first one consisted of a marble-scintillator sampling calorimeter measuring deposited energy and it was followed by a toroidal magnetic spectrometer measuring muon momenta. Later, the CHARM2 detector was an upgraded version of CHARM. Fig. 11 shows the detector, it had a length of 36 m and was followed by a 6 m long magnetic muon spectrometer.

Glass was chosen as a material for the calorimeter because of its low atomic number ($\langle Z \rangle \sim 11$) the accuracy on the electron shower direction measurement being limited by the Z number of the material in which the shower propagates. The "quality factor" is given by:

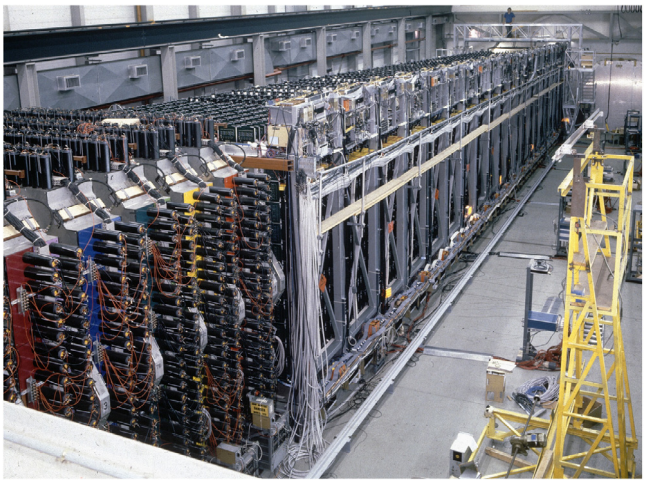

Fig. 11. Photograph of the CHARM2 detector(©CERN).

shower width/shower length $\sim R_{mol}/X^0 \sim Z$

where R_{mol} is the familiar Moliere radius of the shower and X^0 the radiation length of the used material. The accuracy depends further on the sampling frequency.

The full detector consisted of 420 modules of 3.7×3.7 m^2 surface area, each composed of a 4.8 cm thick glass plate ($0.5X^0$) and of a streamer tube plane with 1 cm wire spacing read out at the level of the wires and also by crossed cathode strips 2 cm wide. The total mass was 800 tons for a fiducial mass of 500 tons.

Points along a track could be reconstructed with ± 3 mm accuracy. A shower angular resolution of $\sigma(\theta) \sim 16$ mrad/$\sqrt{(E/\mathrm{GeV})}$ had been achieved for electrons in a calibration test beam.

CHARM2 recognized very well electromagnetic showers and could do measurements complementary to those done by CDHS. In particular it accumulated 1800 elastic scattering of ν_μ and $\bar{\nu_\mu}$ on electrons. With these data it was possible to extract a good measurement of the Weinberg angle:

$\sin^2\theta_W = 0.237 \pm 0.010$.

This result was competitive with other measurements of the same parameter extracted from the ratio M_W/M_Z and from LEP data.

5.5. The NuTeV experiment at Fermilab

NuTeV was a generic neutrino experiment of the calorimeter type built in the Fermilab beam. It consisted of a 690-ton iron-scintillator sampling calorimeter followed by a toroidal muon spectrometer. The front face was 3 m^2, and the overall length was about 40 m. Drift chambers and liquid scintillator counters were interleaved with 10 cm-thick steel plates (about $5\,X^0$) along the length of the calorimeter. The trigger selected events with a penetrating muon and at least 6 GeV of hadronic or electromagnetic energy in the calorimeter. During the 1996–1997 fixed-target run it received 2.5 10^{18} 800 GeV protons on target with half positive and half negative meson focusing. Compared to CDHS the mass is smaller, but this is compensated by the higher beam energy.

The sensitive part was constructed with plastic boxes, filled with scintillation oil, instrumented with a photomultiplier tube looking at each corner. An electrical signal was produced and the signal strength was proportional to the energy deposited by the particle, and thus this acted as a calorimeter. Scintillation counters responded very quickly, allowing to pinpoint accurately the time of a particular event.

Drift chamber planes were used to determine the position of a charged particle passing through. There were 42 of them in the target, and this ensemble could determine the track of a particle, by linking up positions from chamber to chamber. Each chamber had wires at right angles, so that both X and Y positions were measured. As a charged particle passed through the gas in a chamber it ionized some gas molecules. The wire held at a high positive voltage attracted the electrons, and the electrons arriving at the wire produced a signal. The time it took the electron to drift to the wire was proportional to the distance from the wire the particle passed through. The scintillation counter said when the particle passed, so by measuring the time delay before the drift chamber signal, the position was fixed to $\sim$30 μm.

The first part of the detector was followed by the muon spectrometer built around a large toroidal magnet. There were scintillation counters and drift chambers interspersed along the axis of the toroid to track particles passing through the detector. As usual the amount of bend measured the momentum of muons passing through.

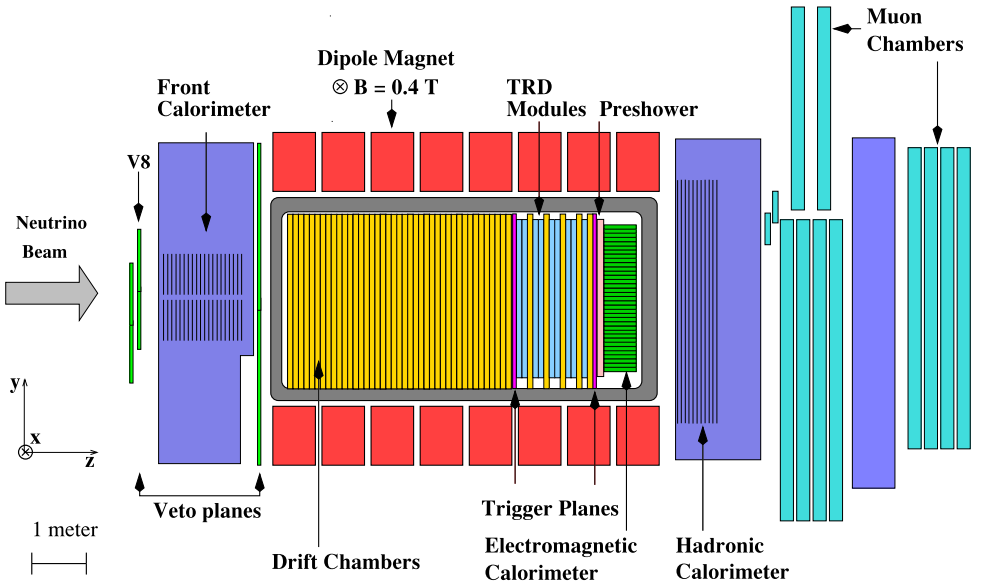

Fig. 12. Schematic view of the NOMAD detector(©CERN).

5.6. The NOMAD experiment at CERN

The NOMAD [44] detector represents a clear evolution in the technique of measuring neutrino interactions. It was located at the CERN WANF and was exposed to the SPS wide-band neutrino beam. During its four years of data taking, 1995–1998, NOMAD collected a total of 2.2 10^{19} 450 GeV protons incident on the target. A view of the detector is shown in Fig. 12.

The apparatus consisted of a number of sub-detectors most of which were located in a large dipole magnet, having an inner volume of 7.5 m along the beam axis and 3.5 $\times$ 3.5 m^2 in crossed dimensions which provided a transverse field of 0.4 T. This magnet was previously used in the UA1 experiment which discovered the W and Z bosons.

Moving downstream along the beam direction came a veto counter, a front calorimeter, a large active target consisting of drift chambers (DC), a transition radiation detector (TRD), a preshower, an electromagnetic calorimeter (ECAL), a hadron calorimeter and an iron filter consisting in the return-yoke of the magnet. The whole apparatus housed in the magnet was followed by a set of large drift chambers used for muon identification. Upstream and downstream of the TRD, two large hodoscopes of scintillators provided a fast trigger. Overall, the detector reconstructed the events kinematics with great precision and identified electrons, muons and photons with high accuracy.

The drift chambers were a crucial part of the detector. They provided the target material and the tracking device for the particles. They were designed with the conflicting requirements that their walls should be as heavy as possible in order to maximize the number of neutrino interactions and as light as possible in order to minimize multiple scattering of particles, secondary particle interactions and photon conversions. To minimize the total number of X^0 for a given target mass, the chambers were made of low density and low atomic number materials. The complete target consisted of 145 drift chambers, with a total mass of 2.9 tons over a fiducial area of 2.6 $\times$ 2.6 m^2. Each chamber contributed 0.02 X^0. Overall, the target had a density of 0.1 g/cm^3, similar to the one of liquid hydrogen, and a total length of 1.0 X^0; there was less than 0.01X^0 between two consecutive hit measurements in the active target. This can be compared with 1.4X^0 in the case of the CDHS detector.

The NOMAD TRD was designed to separate electrons from pions with a pion rejection factor greater than 10^3 for 0.90 electron efficiency in the momentum range from 1 to 50 GeV/c. The ECAL consisted of 875 lead-glass Cerenkov counters arranged in a matrix of 35 rows and 25 columns. The NOMAD muon detector consisted of 10 drift chambers also remnants of the UA1 set-up. Each chamber had an active area of 3.75 $\times$ 5.55 m^2 with two planes in the horizontal and two in the vertical directions for a total of 1210 drift tubes.

In total more than one million neutrino interactions were reconstructed with a precision close to the one obtained with bubble chambers. This allowed the study of precise final state interactions. Figs. 13 and 14 show respectively reconstructed ν_e and ν_μ interactions. In the first case the electron is identified as leaving all its energy in the electromagnetic calorimeter, in the second case a muon is recognized as the charged particle crossing more than 1 m of iron, that is the return yoke of the magnet.

5.7. Dimuon charm cross-sections

The coarse calorimeters of the CDHS type can only measure muons with fair accuracy, and after the DIS studies,the measurements concentrated on events with multiple muons. Fig. 15 shows the record event which reconstructed a total

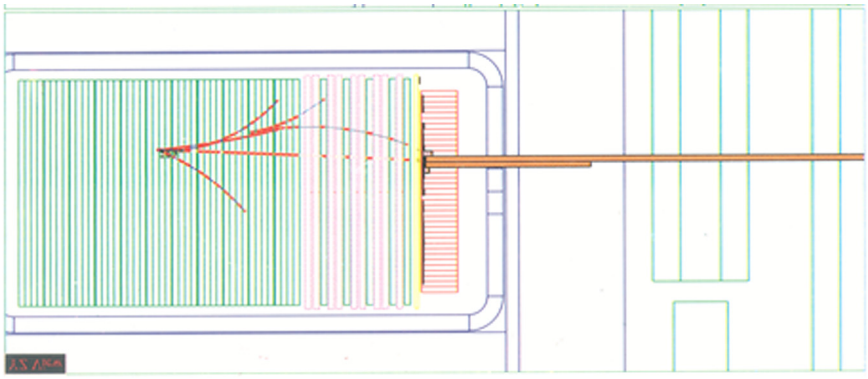

Fig. 13. A reconstructed ν_e interaction in the NOMAD detector(©CERN).

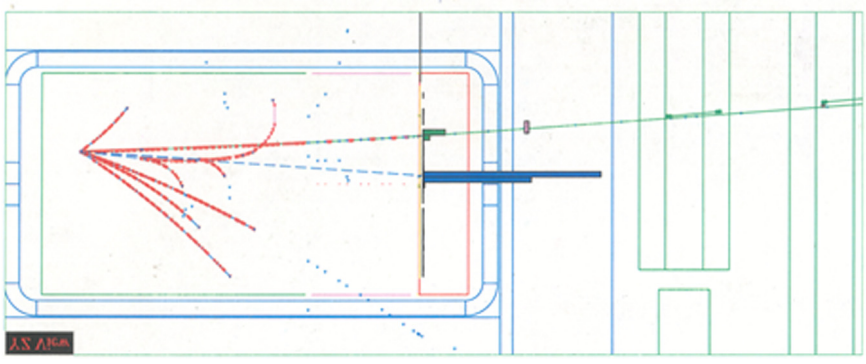

Fig. 14. A reconstructed ν_μ interaction in the NOMAD detector(©CERN).

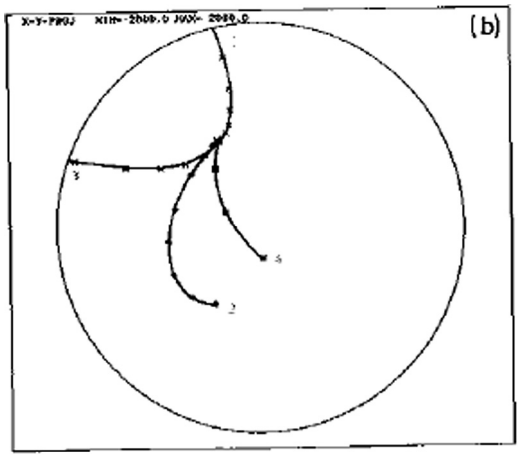

Fig. 15. ν_μ interaction with 4 muons (CDHS back view)(©CERN).

of 4 muons [45]. This was interpreted as coming from simultaneous decays of pions and kaons produced in the interaction. But important physics came with the study of opposite sign dimuons which signaled the production of charm.

The process of opposite sign dimuon production stems from the ν_μ CC production of a charm quark which semileptonically decays into a final state with a secondary muon having an electric charge opposite that of the muon from the primary CC vertex. The DIS production of charm quarks involves the scattering off strange and non-strange quark contents of the nucleon. This allowed to measure in particular the mass of the charm quark.

Neutrinos can produce heavy quark flavors due to the non-diagonal terms in the CC current. The underlying process involved in the production of dimuon events is a neutrino interaction on a *s* or *d* quark. One obtains the following processes:

$$\nu_\mu + d \to \mu^- + c$$
$$\nu_\mu + s \to \mu^- + c$$
$$\bar{\nu_\mu} + \bar{d} \to \mu^+ + \bar{c}$$
$$\bar{\nu_\mu} + \bar{s} \to \mu^+ + \bar{c}$$

with rates proportional to V_{cd}^2 and V_{cs}^2 involving the Cabibbo angle among quarks. The contributions from *d* quarks are suppressed due to the small quark-mixing matrix elements. The generated charm quark evolves in a charmed hadron detected through its semileptonic fast decay. At the level of quarks this corresponds to the semileptonic process:

$$c \to s + \mu^+ + \nu_\mu$$
$$\bar{c} \to \bar{s} + \mu^- + \bar{\nu_\mu}.$$

Charm mesons travel along very small paths (∼mm) before they decay. Thus the final signal consists of two muons of opposite sign coming from a common vertex.

A measurement of the cross section for charm dimuon production in neutrino DIS provides the most direct and clean probe of the strange quark sea content of the nucleon. Large calorimetric type detectors are well adapted to measure this process. Pions and kaons produced in the hadronic shower decay themselves with the emission of muons, but these contributions result in muons of both charges. Thus the corresponding background is directly evaluated from the rate of same-sign dimuons.

The large mass of the charm quark gives rise to a threshold behavior at low energies. This is clearly visible on the data shown in Fig. 16. This behavior allows to fix the charmed quark mass which was found in early experiments to about 1.3 GeV.

Such dimuon investigations have been performed in experiments like CDHS [46], CCFR [47], CHARM2 [48], NuTeV [49] and NOMAD [50]. Because of its lowest energy threshold, $E_\nu \sim 6$ GeV, and its high resolution, NOMAD reached a new level of precision in this measurement. Furthermore, the neutrino spectrum in NOMAD was well suited to study charm production; being close to the charm threshold it provided enhanced sensitivity to the charm production parameters.

In this measurement, the FCAL was used as the interaction target to profit from its large mass. The selection of the events required two muons accurately analyzed in the DC region and well recognized in the muon system. Such a signal selected opposite sign dimuons and like sign dimuons for background estimation. The total hadronic energy was calculated with both the energy measured in the FCAL and subsequently measured in the DC's. The selection was based on a primary muon (the highest energy one) of negative charge, thus suppressing the contribution of antineutrino interactions.

The background was evaluated from the $\mu^-\mu^-$ events corrected by a scale factor extracted from the MC. The background estimate was checked using the data themselves consisting in mesons of both charges detected in the DC's. After all cuts, the analysis retained 20 479 opposite sign dimuons of which 75 10^{-2} were genuine charm signal. This represented the highest available statistics, and the quality of the reconstruction allowed to lower significantly the energy threshold on the second muon down to 3 GeV. The analysis measured the ratio of the charm dimuon cross-section to the inclusive CC cross-section as a function of the kinematic variables:

$$R_{\mu\mu} = \sigma_{\mu\mu}/\sigma_{CC} \sim N_{\mu\mu}/N_{CC}.$$

By integrating this result, the average dimuon production in NOMAD was evaluated. Over the NOMAD flux, for $Q^2 \geq 1\ \mathrm{GeV}^2/c^2$, the result was: $(5.15 \pm 0.05 \pm 0.07)\ 10^{-3}$. The first uncertainty is statistical, the second systematic. By fitting $R_{\mu\mu}$ it was possible to extract the charm production parameters including the mass of the charm quark and the effective semileptonic branching ratio B_μ. The running mass of the charm quark was found to be:

$$m_c = (1.159 \pm 0.075)\ \mathrm{GeV/c^2}.$$

The semileptonic branching ratio was parameterized as a function of the neutrino energy:

$$B_\mu(E_\mu) = \frac{0.097 \pm 0.003}{1 + (6.7 \pm 1.8)/E_\mu}.$$

These results represent the most precise measurements from neutrino data.

Charm has also been detected by direct search for D^0 production. In their emulsions CHORUS found 283 candidates for an expected background of 9 [51]. Also NOMAD found 35 events compatible with the production of D^{*+} using the decay chain $D^{*+} \to D^0 + \pi^+$ followed by $D^0 \to K^- + \pi^+$ [52].

5.8. Extraction of structure functions

Following the formalism introduced before, DIS processes can be completely described in terms of three dimensionless kinematic invariants, the inelasticity *y*, the Bjorken *x* and the 4-momentum transfer $Q^2 = -q^2$, where $q = p_\nu - p_\mu$.

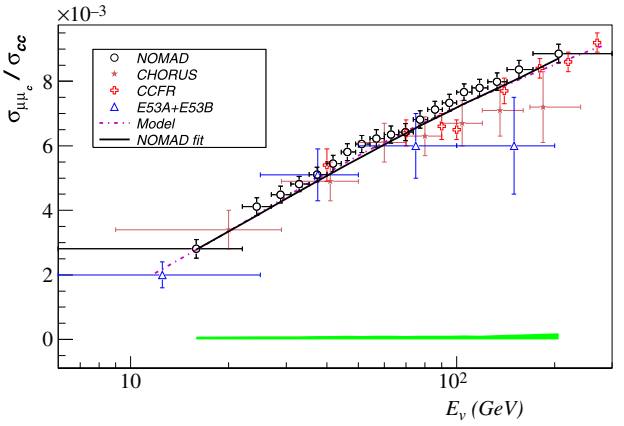

Fig. 16. Ratio of dimuon over single muon rates as a function of E_ν.

On a practical level these Lorentz-invariant parameters can be reconstructed using readily measured observables:

$$Q^2 = -m_\mu^2 + 2E_\nu(E_\mu - p_\mu \cos\theta)$$
$$x = \frac{Q^2}{2p_\mu q} = \frac{Q^2}{2ME_{had}}$$
$$y = \frac{E_{had}}{E_\nu}$$

where the quantities directly measured by the experiments are E_μ, p_μ and θ, the energy, momentum and scattering angle of the outgoing muon in the laboratory frame. E_ν is also measured by the kinematics of the event or by reconstruction of the impact point for narrow band beams experiments. In the case of NC events, the outgoing neutrino is not reconstructed, all of the event information is inferred from the hadronic shower and the beam direction.

Using these variables the inclusive cross section for DIS of neutrinos and antineutrinos is:

$$\frac{d^2\sigma}{dxdy} = \frac{G^2ME_\nu}{\pi(1+Q^2/M_B^2)^2}[y^2xF_1(x,Q^2) + (1-y-Mxy/2E)F_2(x,Q^2) \pm y(1-y/2)xF_3(x,Q^2)]$$

where the $\pm$ sign is $+$ for neutrinos and $-$ for antineutrinos, and the mass M_B is the $W^\pm$ mass for CC and the Z^0 mass for NC currents.

In the above expression, F_i are the dimensionless nucleon structure functions. In the case of electron scattering there are two structure functions while for neutrino scattering there is the additional F_3 parameter which represents the V–A interference term.

Assuming the quark parton model, the structure functions can be expressed in terms of the quark composition of the target. They depend on the target and type of scattering, either NC or CC, and are functions of x and Q^2. The nucleon structure functions can be expressed as the sum of the probabilities over the different quark flavors found in the hadrons:

$$F_2(x,Q^2) = 2\sum_{i=u,d\ldots}[xq(x,Q^2) + x\bar{q}(x,Q^2)]$$
$$xF_3(x,Q^2) = 2\sum_{i=u,d\ldots}[xq(x,Q^2) - x\bar{q}(x,Q^2)].$$

The struck quark carries a fraction x of the nucleon momentum such that xq is the probability to find a quark of flavor q with a given momentum fraction, and $x\bar{q}$ is the same for antiquarks. In this way F_2 measures the sum of quarks and antiquarks pdf's present in the nucleon while xF_3 measures their difference. It is then possible to extract directly the pdf's content of the valence quarks. The third structure function $2xF_1$ is commonly related to F_2.

Measurements of these structure functions have been the focus of many DIS experiments. Neutrino scattering is unique in that it measures the valence quark distributions through xF_3 but also the strange quark distribution through detection of neutrino-induced dimuon production. This provides important constraints that cannot be obtained from either electron or muon scattering experiments.

Experimentally the structure functions are determined from the differential cross sections. From these, the single-quark distribution functions as well as the gluon structure functions $xg(x)$ can be extracted. Fig. 17 shows a compilation of x distributions obtained with increasing energies. Two of them come from neutrino scattering (Gargamelle and CDHS) and

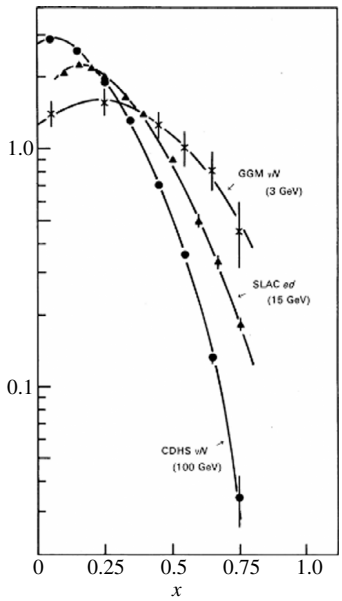

Fig. 17. x distributions obtained at various energies.

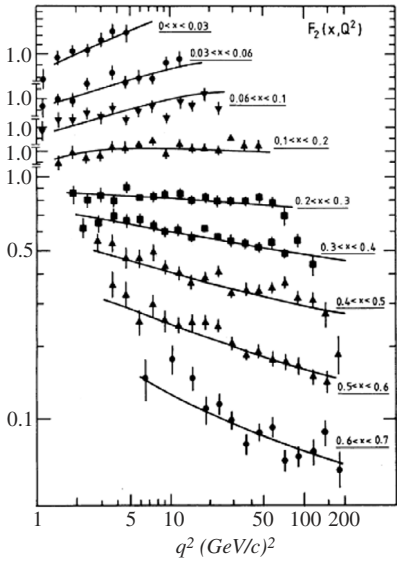

Fig. 18. Structure function F_2 for various x values.

they are compared with the same distribution coming from electron–proton scattering (SLAC). The x variation is more peaked at higher energies.

The results are given for a fixed Q^2. But over a wide range of Q^2 it was found that structure functions show a deviation from the simple scaling at fixed x. Fig. 18 shows the variation of the same F_2 structure function as a function of Q^2 [4]. In these plots scaling means that for a given x the cross sections do not vary with Q^2. Consequently the plots should appear as horizontal lines. What is found is that the structure functions show a deviation from scaling, namely a variation as a function of Q^2 for a fixed x. As Q^2 increases, F_2 rises at small x and gets smaller at high x.

This can be understood within the framework of QCD. Higher Q^2 implies a better time and spatial resolution. More and more partons from the sea can be observed with smaller momentum fractions leading to a rise at small x. The Q^2 evolutions of the structure functions are described by the DGLAP equations (Dokshitzer, Lipatov, Altarelli and Parisi) [53–55]. Fig. 18 clearly tells us that the observed quark distributions vary with Q^2. The sea quarks are concentrated at low x values, while the valence quarks extend to higher values.

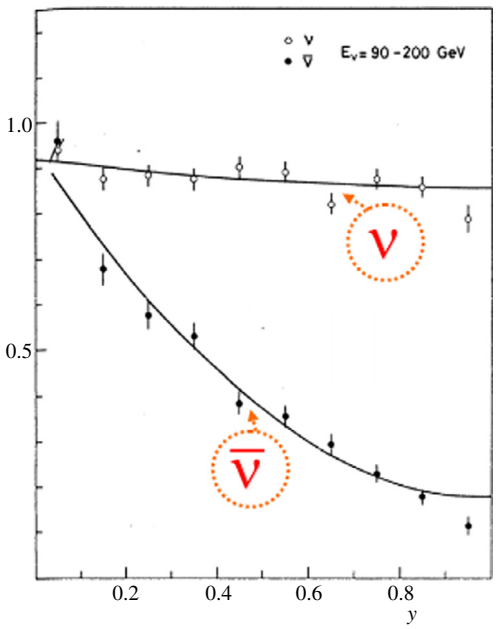

Fig. 19. Differential cross section versus y.

The y distributions will give the quark content from the total cross section. This is explained as follows: the fraction of the proton momentum carried by u-quarks is defined by:

$$U = \int_0^1 xu(x)dx$$

and in a similar way for other quarks. Using this notation, the y distributions are then given by:

$$d\sigma(\nu N) \sim [q + \bar{q}(1-y)^2]$$
$$d\sigma(\bar{\nu} N) \sim [q(1-y)^2 + \bar{q}].$$

Neglecting s and c contributions, the ratio of both y distributions is approximately 1 for $y = 0$. Fig. 19 shows the corresponding y distributions from the CDHS experiment [56].

From these plots one extracts:

$$\frac{\bar{q}}{q+\bar{q}} = 0.15 \pm 0.03$$
$$\frac{\bar{s}}{q+\bar{q}} = 0.00 \pm 0.03$$
$$\frac{\bar{q}+s}{q+\bar{q}} = 0.16 \pm 0.01.$$

After integration with respect to y the total cross sections become:

$$\sigma(\nu N) \sim \frac{\sigma_0}{3}[3q + \bar{q}]$$
$$\sigma(\bar{\nu} N) \sim \frac{\sigma_0}{3}[q + 3\bar{q}].$$

Defining the ratio $R = \sigma(\nu N)/\sigma(\bar{\nu} N)$, it results:

$$\frac{\bar{q}}{q} = \frac{3-R}{3R-1}.$$

The experimental value of R is $R \sim 2.02$. From this it follows that $q \sim 0.41$ and $\bar{q} \sim 0.08$.

Therefore one can extract the contributions from valence and sea quarks separately. They amount respectively to:

$q_V = q - \bar{q} \sim 0.33$ and $s = \bar{s} = \bar{q} \sim 0.08$.

This shows that quarks and antiquarks carry about 0.49 of the proton momentum whereas valence quarks alone contribute about 0.33 and sea quarks 0.16. Half of the proton momentum has to be carried by the gluons which do not interact with the neutrinos [57].

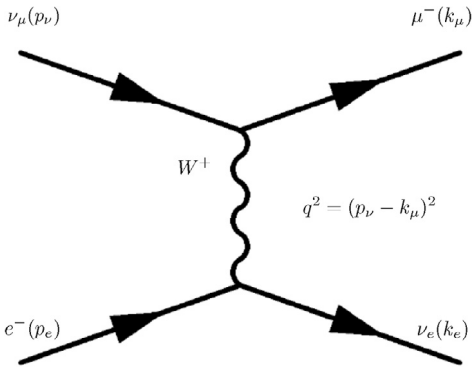

Fig. 20. Feynman diagram for inverse muon decay.

5.9. High energy neutrino–electron elastic scattering

As was explained before, the totally leptonic process:

$$\nu_\mu + e^- \longrightarrow \nu_\mu + e^-$$

is crucial to check the theory. Experimentally a single electron is produced and the problem is to clearly identify it. Large calorimeters give an adequate identification of muons which travel over meters in matter, but the signature of electrons is different. Electrons shower in a depth of about 10 X^0. In DIS events, π^0 are copiously produced and give photons which show a signature similar to the one given by single electrons. In order to identify the elastic channel it is essential to have a detector with a good identification of the electron and a good measurement of its energy. This is the scope of a fine grained apparatus highly segmented in the region surrounding the interaction vertex. CDHS had a too coarse granularity to give a signal precise enough. This is why, in parallel with the CDHS detector a second experiment took data, the CHARM one. It had a smaller total mass but enjoyed a finer granularity which allowed a clean identification of single electrons. Later CHARM2 reported the largest sample of 762 $\nu_\mu e^-$ events and 1017 $\bar{\nu}_\mu e^-$ events [58].

The main goal of studying these reactions was to determine the parameters of the SM with highest precision, in particular $g_A = -1/2$ and $g_V = -1/2 + 2\sin^2(\theta_W)$ of the electron.

The results were:

$$g_A = -0.525 \pm 0.032$$
$$g_V = 0.036 \pm 0.018.$$

This contributed to a test of the electroweak theory and proved in good agreement with the more precise measurements of LEP.

5.10. Inverse muon decay

The CHARM experiment also measured the inverse muon decay channel [59]:

$$\nu_\mu + e^- \longrightarrow \mu^- + \nu_e.$$

We have already introduced the muon decay:

$$\mu^- \longrightarrow e^- + \nu_\mu + \bar{\nu_e}.$$

The same exchange applies to understand the interaction of ν_μ with atomic electrons. The graph is shown in Fig. 20.

The only visible particle produced in the interaction is a muon. The reaction is characterized by a threshold at 10.8 GeV because of the muon mass. The signature is simple, it requires no detectable recoil energy at the vertex point and the forward emission of the muon is at small angles ($\theta_\mu \leq 10$ mrad).

But in order to be sure of the right identification it is essential to check that no accompanying track is produced. The extraction of the signal requires a high granularity around the vertex.

Using again the variables w and y, one finds the cross sections:

$$\frac{d\sigma(\nu_\mu + e^- \longrightarrow \mu^- + \nu_e)}{dy} = \frac{2mwG_W(t)^2}{\pi\left[1 - \frac{m_\mu^2 - m_e^2}{2wm_e}\right]}.$$

Neglecting the lepton masses this gives the total cross section for ν_μ inverse muon decay:

$$d\sigma(\nu_\mu + e^- \longrightarrow \mu^- + \nu_e) = 2mwG^2/\pi$$

with $2mG^2/\pi \sim 15.3\ 10^{-42}$ cm^2/GeV.

Inverse muon decay is similarly open to incident $\bar{\nu}_e$, and one finds:

$$d\sigma(\bar{\nu}_e + e^- \longrightarrow \mu^- + \bar{\nu_\mu}) = 2mwG^2/3\pi.$$

The factor 1/3 is typical of the antifermion–fermion scattering in a V–A theory.

With a statistics of about 15 000 candidate events CHARM2 measured a cross section for the inverse muon decay of:

$$\sigma = 17.9\ 10^{-42} E\ \text{cm}^2.$$

The ratio of the elastic process over the inverse muon decay cross sections gives an interesting result:

$$\sigma(\nu_\mu e^- \longrightarrow \nu_\mu e^-)/\sigma(\nu_\mu e^- \longrightarrow \mu^- \nu_e) = \rho^2(1/4 - \sin^2\theta_W + 4/3\sin^4\theta_W).$$

In the ratio some of the systematics disappear and this allowed to extract the Weinberg angle and the ρ parameter introduced in the overview of the theory with good precision:

$$\sin^2\theta_W = 0.24 \pm 0.02$$
$$\rho = 0.977 \pm 0.045.$$

5.11. Neutrinos and the Weinberg angle

The parameter $\sin^2(\theta_W)$ depends only very weakly on the top and Higgs masses. A precise determination is obtained from DIS on (approximately) isoscalar targets by comparing the cross sections of CC's and NC's. The ratio R_ν of NC/CC cross sections has been measured by CDHS [60] and CHARM [61] collaborations and CCFR has obtained even more precise results [62]. Most of the uncertainties from strong interactions and neutrino spectra cancel in the ratio.

A simple approximation gives:

$$R_\nu = g_L^2 + g_R^2 r$$
$$R_{\bar{\nu}} = g_L^2 + g_R^2/r$$

where:

$$g_L^2 \sim 1/2 - \sin^2(\theta_W) + 5/9\sin^4(\theta_W)$$
$$g_R^2 \sim 5/9\sin^4(\theta_W)$$

with the parameter r being the ratio $CC_{\bar{\nu}}/CC_\nu$ measured directly by experiments. In the simple parton model $r = (1/3 + \epsilon)/(1 + 1/3\epsilon)$ where $\epsilon \sim 0.12$ is the ratio of the fraction of the nucleon momentum carried by antiquarks to that carried by quarks.

Combining all of the precise DIS measurements one obtains:

$$\sin^2(\theta_W) = 0.2260 \pm 0.0039.$$

This is in agreement with more precise determinations of $\sin^2(\theta_W)$ coming in particular from LEP data. With Standard Model assumptions, this measurement of $\sin^2(\theta_W)$ indirectly determines the W boson mass to a precision comparable to direct measurements from high energy e^+e^- and $p\bar{p}$ colliders.

But a more recent result coming from the NuTeV experiment has remeasured the Weinberg parameter with neutrinos and found a tension with previous results [63].

The measurement of NuTeV is:

$$\sin^2\theta_W = 0.2253 \pm 0.0019(\text{stat}) \pm 0.0010(\text{syst})$$

which implies $M_W = 80.26 \pm 0.11$ GeV. This result is higher than the Standard Model prediction obtained from LEP experiments. The discrepancy is at the level of $5\ 10^{-3}$. This anomaly is still not resolved, it could be explained in terms of oscillations of ν_e into sterile neutrinos ν_H [64]. This interpretation implies a transition probability $\nu_e \to \nu_H$ at the level of $(0.21 \pm 0.07)10^{-2}$. Such a probability is compatible with other neutrino data if the mass-squared difference that drives the oscillation is in the range $\delta m^2 \sim$ 10–100 eV^2/c^4. We will come back later to the problem of neutrino masses.

5.12. Study of quasi-elastic events

QE scattering is predominant at energies up to ∼2 GeV, but it remains present even with high energy neutrinos. To study such a channel, it is necessary to have a fine-grained detector. Bubble chambers would have been ideal, but the searched-for process is rare and their repetition rate is much too low to accumulate a large number of events. With its high granularity target NOMAD was well suited to study the ν_μ QE scattering reaction where the target neutron is converted to a proton:

$$\nu_\mu n \longrightarrow \mu^- p.$$

A high energy beam has a sizable contribution of antineutrinos, so that the experiment also measured the conversion of a proton into a neutron:

$$\bar{\nu_\mu} p \longrightarrow \mu^+ n.$$

The cross section for these processes depends on the vector, axial–vector and pseudoscalar form factors which are present in the hadronic weak current. In practice, the pseudoscalar contribution is typically neglected as it enters the cross section multiplied by the very small factor m^2/M^2. The vector form factor is obtained from electron scattering, thus leaving the neutrino experiments with the task to measuring the axial–vector form factor of the nucleon $F_A(Q^2)$. This factor is parameterized with only one adjustable parameter the so-called axial mass M_A. This number describes the internal structure of the nucleon and should be the same both for neutrino and antineutrino measurements. It is customary to assume a dipole form:

$$F_A(Q^2) = \frac{g_A}{[1 + Q^2/M_A^2]}.$$

Thus the form factor depends on two empirical parameters: its value at $Q^2 = 0$ and M_A. $F_A(0) = g_A$ is very well known from nuclear beta decay [65]. The result is $g_A = 1.2694 \pm 0.0028$. The only unknown remains M_A.

Early measurements driven by deuterium targets in bubble chambers gave values of M_A ranging from 0.65 to 1.09 GeV. They suffered from small statistics. Moreover large systematic uncertainties came from the poor knowledge of the incoming neutrino flux. Modern day experiments use more complex nuclei. As a result nuclear effects become more important. The nucleus is typically described in terms of individual quasi-free nucleons that participate in the scattering process. Analyzing higher statistics and using a Fermi-gas model, modern experiments have repeated the measurement. Most of them find higher M_A values than those coming from the deuterium fits. Axial mass values from 1.05 to 1.35 GeV have been obtained [66,67]. This discrepancy has sparked new interest. The assumed dipole form chosen for the axial vector form factor is an ansatz, but it is known that the vector form factor obtained from the more precise electron scattering shows a significantly more complicated dependence on Q^2. Fig. 21 summarizes the existing measurements of ν_μ QE scattering cross sections as a function of neutrino energies. As expected the cross section rises linearly until it is damped by the form factors at higher energies.

For example NOMAD used a sample of 751 000 ν_μ CC events in a reduced fiducial volume, the average energy of the incoming ν_μ being 25 GeV. The event selection retained two tracks originating from the primary vertex, one of them identified as a muon. The muon track was easily reconstructed, however the proton was more difficult to measure. Sometimes the proton could not be properly reconstructed because its momentum was too low, well below 1 GeV/c, or its angle too large, above 60°. For positive tracks such conditions meant that they made almost immediately a U-turn under the magnetic field.

Moreover the tracks were in the $1/\beta^2$ region of ionization loss and they crossed the drift cells at very large angles where the spatial resolution of the DC's was considerably worse. Some of these effects were difficult to simulate. Also the proton could lose part of its energy in an intranuclear cascade. In the analysis it was important to disentangle the reconstruction efficiency effects from the effects induced by intranuclear cascade which changed the proton kinematics. Using only 2-track events did not alleviate the problem of a large systematic uncertainty coming from insufficient understanding of nuclear effects. To increase the statistics and alleviate some of the difficulties, the 1-track sample, muon only, was also used. For these events the muon momentum and direction were the sole measurements and conservation laws were used to compute other kinematical quantities like E_ν and Q^2.

In total the samples used in the analysis consisted of 14 021 neutrino and 2237 antineutrino events. No precise knowledge of the integrated neutrino flux existed, so the QE cross section was normalized to the total DIS ν_μ CC cross section or to inverse muon decay. The flux-averaged QE cross section was measured in the neutrino energy region 3–100 GeV. The result for ν_μ was:

$$\sigma_{QE} = (0.92 \pm 0.02(\text{stat}) \pm 0.06(\text{syst}))10^{-38}\ \text{cm}^2$$

and for $\bar{\nu_\mu}$:

$$\sigma_{QE} = (0.81 \pm 0.05(\text{stat}) \pm 0.09(\text{syst}))10^{-38}\ \text{cm}^2.$$

The axial mass was extracted and the result for neutrino data was:

$$M_A = [1.05 \pm 0.02(\text{stat}) \pm 0.06(\text{syst})]\ \text{GeV}.$$

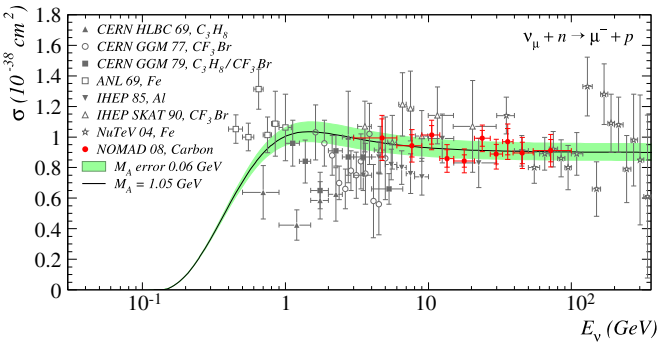

Fig. 21. ν_μ QE scattering cross sections as a function of energy.

For the antineutrino data the result was:

$$M_A = [1.06 \pm 0.07(\text{stat}) \pm 0.12(\text{syst})]\ \text{GeV}.$$

Given that the newly appreciated effects of nucleon–nucleon correlations are expected to be different for neutrinos and antineutrinos, the study of antineutrino QE scattering at low energies is important. Unfortunately, no current measurement exists below 1 GeV. Also direct measurements of ν_e or $\bar{\nu}_e$ QE cross sections have yet to be performed.

NC elastic scatterings corresponding to the channels:
$\nu_\mu p \longrightarrow \nu_\mu p$, $\nu_\mu n \longrightarrow \nu_\mu n$, $\bar{\nu_\mu} p \longrightarrow \bar{\nu_\mu} p$, $\bar{\nu_\mu} n \longrightarrow \bar{\nu_\mu} n$,
have also been measured but with a much coarser precision [68].

5.13. Coherent pion production

Neutrinos can also coherently produce a single pion in the final state. In this case, the neutrino scatters off the entire nucleus, transferring negligible energy to the target. Fig. 22 shows the corresponding diagram in the case of the π^0 production. No charge or isospin is exchanged between the neutrino and the nucleon in the target. These low Q^2 interactions produce no measurable nuclear recoil and a distinctly forward-scattered pion, compared to their resonance-mediated counterparts. Both NC and CC coherent pion production processes are possible:
$\nu_\mu A \longrightarrow \nu_\mu A\pi^0$, $\nu_\mu A \longrightarrow \mu^- A\pi^+$, $\bar{\nu_\mu} A \longrightarrow \bar{\nu_\mu} A\pi^0$, $\bar{\nu_\mu} A \longrightarrow \mu^+ A\pi^-$.

While the cross sections for these processes are predicted to be comparatively small, coherent pion production has been observed across a broad energy range in both NC and CC interactions of neutrinos and antineutrinos. Most of these historical measurements were performed at energies $E_\nu \geq 2$ GeV. More recent measurements of coherent pion production from a variety of nuclear targets come from K2K [69], MiniBooNE [70] and NOMAD [71].

Experiments measuring coherent pion production at very low neutrino energies have typically observed less coherent pion production than predicted by models which describe well the high energy data. To date, it has been a challenge to develop a single description that can successfully describe existing measurements across all energies. The most common theoretical approach for describing coherent pion production is typically based on Adler's PCAC theorem [72] which relates neutrino-induced coherent pion production to pion–nucleus elastic scattering in the limit $Q^2 = 0$. A nuclear form factor is then invoked to extrapolate to non-zero values of Q^2. Such PCAC-based models [73] have existed for many years and have been rather successful in describing coherent pion production at high energy.

5.14. Strange particles production

Neutrino interactions can also produce final states involving strange quarks. These reactions typically have small cross sections due in part to the kaon mass and also because kaon channels are not enhanced by any dominant resonance. Very few experiments have published data on charged kaon production because the identification of such particles require special identification hardware, for example RICH counters which would be too cumbersome to install in a neutrino detector.

All previous investigation of strange particle production by neutrinos came from bubble chamber experiments which suffered from low statistics. Recently a number of NOMAD publications dealt with strangeness production relying on the excellent reconstruction of neutral strange particles through their decays. Production yields and multiplicities for a variety of reaction kinematics have been published [74–76]. First, the inclusive yields of strange particles were measured. This gave a useful testing ground for the quark–parton model and for hadronization processes.

Neutral strange particles were reliably identified using the V^0-like signature of their decay products. Among the 1.3 10^6 ν_μ CC events collected, the NOMAD experiment observed an unprecedented number of neutral particle decays appearing as a V^0-like vertex in the detector with an excellent reconstruction quality. The order of magnitude increase in statistics was

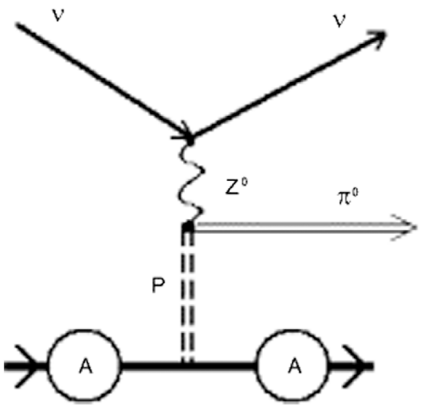

Fig. 22. Coherent pion production diagram.

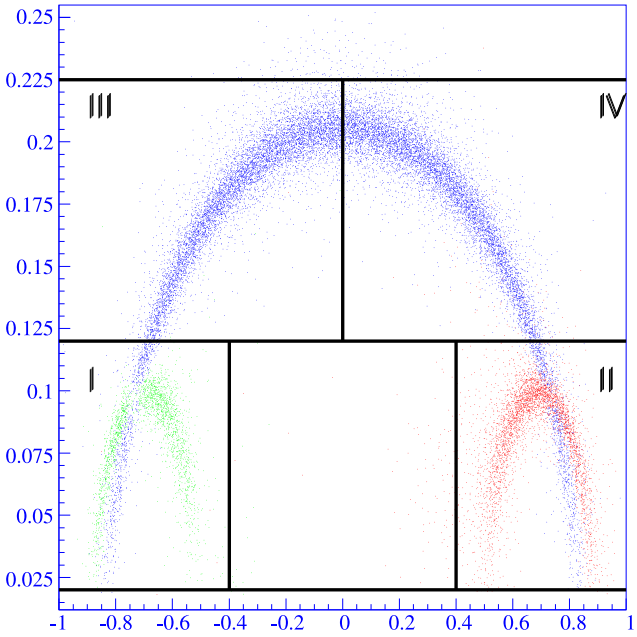

Fig. 23. Plot of p_T^{int} vs. α as explained in the text.

used to improve the knowledge of K_s, Λ, $K^{*\pm}$, $\Sigma^{*\pm}$, Σ^0 and $\Xi^{\pm}$ production in ν_μ CC interactions. Furthermore this study allowed a quantitative theoretical interpretation of the Λ polarization measurements.

Since NOMAD was unable to distinguish protons from pions in the momentum range of the analysis, the V^0 identification procedure relied on the kinematic properties of the V^0 decay. The fit method was performed for three decay hypotheses: $K_s \to \pi^+ + \pi^-$, $\Lambda \to p + \pi^-$ and $\bar{\Lambda} \to \bar{p} + \pi^+$ and for the hypothesis of a gamma conversion to e^+e^-.

Fig. 23 shows the plot obtained for p_T^{int} vs. α in data events, where p_T^{int} is the transverse component of one of the outgoing charged tracks with respect to the V^0 momentum, and $\alpha = \frac{p_L^+ - p_L^-}{p_L^+ + p_L^-}$ is the longitudinal momentum asymmetry between the positive and negative tracks.

Different regions of the plot correspond to different populations. Three regions corresponding to K_s, Λ and $\bar{\Lambda}$ are clearly visible, with the K_s sample being symmetric under α, while $\bar{\Lambda}$'s and Λ's populate boxes I and II respectively. Photon conversions populate the small p_T^{int} region.

Identified V^0 were of two types:

– uniquely identified V^0, which populated regions in which decays of only a single particle type was present,

– ambiguously identified V^0 which populated regions in which decays of different particle types were present.

It was possible to select subsamples of uniquely identified V^0's with high purity: 0.98 for K_s, 0.97 for Λ and 0.90 for $\bar{\Lambda}$. The treatment of ambiguities aimed at selecting a given V^0 decay with the highest efficiency and the lowest background contamination from other V^0 types.

The total V^0 sample contained 15 074 identified K_s, 8987 identified Λ and 649 identified $\bar{\Lambda}$, representing significantly larger numbers with respect to previous experiments done with bubble chambers. Thus the production rate of neutral strange particles in ν_μ CC interactions was measured. The integral yields per ν_μ CC interactions were the following:

$(6.76 \pm 0.06)10^{-2}$ for K_s, $(5.04 \pm 0.06)10^{-2}$ for Λ and $(0.37 \pm 0.02)10^{-2}$ for $\bar{\Lambda}$.

The yield of K_s rose steadily with E_ν and w^2, reaching a plateau at large Q^2 and falling with increasing Bjorken x. The Λ yield showed a behavior almost independent of E_ν, w^2 and Q^2 after a sharp initial rise. The smaller $\bar{\Lambda}$ yield was measured for the first time.

Furthermore, a detailed analysis of kinematic quantities describing the behavior of neutral strange particles inside the hadronic jet was performed. In particular, the following distributions were studied:

– the Feynman x_F, the longitudinal momentum fraction in the hadronic center-of-mass system;

– the fraction $z = E_{lab}(V^0)/E_{lab}(allhad)$ of the hadronic energy carried away by the neutral strange particle in the laboratory system;

– the transverse momentum squared p_T^2, of a particle with respect to the hadronic jet direction.

The x_F distribution indicated that Λ's were produced mainly in the target fragmentation region ($x_F \leq 0$) while K_s were peaked in the central region with an asymmetry in the forward direction. $\bar{\Lambda}$'s were produced in the central x_F region ($-0.5 \leq x_F \leq 0.5$). The z distributions showed a turnover at small values for $\bar{\Lambda}$'s but not for K_s and Λ's showed a maximum at z going to 0.

5.15. Inclusive resonance production

An interaction channel which has been carefully studied is the low multiplicity resonance production. Also here the contribution of NOMAD was essential. The experiment was able to measure the production yield of meson resonances $\rho^0(770)$, $f_0(980)$ and $f_2(1270)$ [77]. In particular the f_0 meson was observed for the first time in neutrino interactions.

All combinations of tracks with momenta larger than 0.1 GeV/c originating at the primary vertex and not identified as electrons or muons were used for the reconstruction of the resonance candidates. All used tracks were assigned the pion mass. The distribution of the $\pi^+\pi^-$ invariant mass showed an enhancement at the ρ^0 mass which was not present in the like-sign distribution. When a cut $x_F \geq 0.6$ was applied to reduce the combinatorial background, clear peaks at the f_0 and f_2 masses were visible. The resonance signal was determined by fitting the invariant mass distribution to a sum of relativistic Breit–Wigner functions with combinatorial background added. The average $\rho^0(770)$ multiplicity measured for ν_μ CC interactions was found to be $(0.195 \pm 0.007 \pm 0.019)$ for $w \geq 2$ GeV. It was similar in $\bar{\nu_\mu}$ CC interactions.

NOMAD also measured the production of strange resonances and heavier hyperons. This study was of interest for the theoretical interpretation of Λ and $\bar{\Lambda}$ polarization measurements. This was essential because Λ's originating from the decays of Σ^*, Σ^0 and Ξ^0, inherit a polarization from their parent particles different from that of a directly produced Λ.

To construct the samples, neutral strange particles were combined with all possible charged tracks of appropriate sign emerging from the primary vertex except those identified as muons or electrons. Combinations of Λ with γ were also studied, where photons were identified as e^+e^- conversions in the detector fiducial volume. The $K^{*\pm}$ was recognized in the $K_s\,\pi^\pm$ invariant mass distributions, the $\Sigma^{*\pm}$ appeared in the $\Lambda\pi^\pm$ combinations. Still in the $\Lambda\pi^-$ there was evidence of Ξ^- production. Similarly Ξ^0 showed in the invariant mass distribution of $\Lambda\gamma$ combinations.

Corrected fractions of observed K_s and Λ decays that originated from the decays of strange resonances and heavy hyperons were found to be: $(15.5 \pm 0.9)10^{-2}$, $(8.7 \pm 0.7)10^{-2}$, $(5.8 \pm 1.1)10^{-2}$, $(2.6 \pm 0.8)10^{-2}$, $(7.3 \pm 2.4)10^{-2}$ and $(1.9 \pm 1.7)10^{-2}$ for the channels: $K^{*+} \to K_s\pi^+$, $K^{*-} \to K_s\pi^-$, $\Sigma^{*+} \to \Lambda\pi^+$, $\Sigma^{*-} \to \Lambda\pi^-$, $\Sigma^0 \to \Lambda\gamma$, $\Xi^- \to \Lambda\pi^-$ respectively.

5.16. The OPERA detector

We have described a series of important neutrino detectors offering granularities from the coarse to the very fine. They allowed to study many diverse channels and this applied essentially to the case of ν_μ which is by far the dominant species present in accelerator beams. ν_e interactions have also been studied thoroughly but with less precision because of lower statistics.

But we know of the existence of a third type of neutrino, the ν_τ. At a certain point in the progress of neutrino physics, it became compulsory to check the universality of neutrino interactions by detecting direct interactions of this ν_τ. This was done a first time with the DONUT experiment at Fermilab to prove the existence of this third neutrino type. A few events were registered in agreement with expectations. More recently, the OPERA experiment [78] had the task to check directly ν_μ oscillations by checking the appearance of ν_τ in an originally pure ν_μ beam.

A ν_τ interaction is characterized by a very special signature and requires a dedicated technique. The reason is that to recognize such a CC interaction it is necessary to sign the production of a τ lepton. Such a particle, because of its mass, has a very small lifetime, 2.910^{-13} s. At the energies available at present accelerators, the τ decays after a path of 1 mm in average. This gives a very short track and the detectors described so far do not have the required spatial resolution. There are few

Fig. 24. One tau-decay event seen in the OPERA detector (©CERN).

media allowing such a precision on measuring a track, even bubble chambers were not precise enough. The idea was to use photographic emulsions where tracks can be followed with $\sim$10 μm spatial accuracy.

The OPERA experiment was positioned in the CERN ν_μ beam, but at the large distance of 730 km from the source, housed in the underground Hall C of the Gran Sasso Laboratory near Rome. The set-up was modular, the tracks resulting from the interaction of a ν_τ were produced in target units called bricks made of nuclear emulsion films interleaved with lead plates. The OPERA target contained 150 000 such bricks, for a total mass of 1.25 kton, arranged into walls interleaved with plastic scintillator strips. The detector was split into two identical supermodules, each supermodule containing a target section followed by a magnetic spectrometer for momentum and charge measurement of penetrating particles, namely muons. Real time information from the scintillators and the spectrometers provided the identification of the bricks where the neutrino interactions occurred. When a possible interaction was registered, the candidate brick was extracted from the walls and, after X-ray marking and an exposure to cosmic rays for alignment, their emulsion films were developed and sent to the emulsion laboratories to perform a complicated scanning procedure in order to extract information on the event.

The construction of the detector started in 2003 and it was completed in summer 2008. The experiment is now ended. The whole sequence of operations has proven to be successful, from triggering to brick selection, development, scanning and event analysis, and the experiment has ended its data taking succeeding in finally recognizing 5 ν_τ events in full agreement with oscillation expectations. Fig. 24 shows a tau-decay event reconstructed in the OPERA detector. It was recognized as a decay $\tau^- \to \nu_\tau h^-$.

This small statistics was enough to reject the no-oscillation scenario at a 5σ C.L.

5.17. Backward going particles

In high energy interactions off nuclei there are particles emitted backwards with respect to the beam direction which have energies not allowed by the kinematics of collisions on a free and stationary nucleon. Backward going protons are commonly observed while their production is forbidden in absence of nuclear effects. Likewise, high energy mesons are detected at momenta above the kinematical limit. These effects have been used to investigate the nuclear structure of the target. Two categories of models are proposed to explain the origin of these particle productions:

– In the intranuclear cascade models, the production of particles in the kinematically forbidden region can be seen as the result of multiple scattering and of interactions of secondary hadrons produced in the primary ν-nucleon collision, while they propagate through the nucleus. One observes that the cascade is restricted to slow particles only, while the fast ones do not reinteract inside the nucleus. The currently accepted explanation for this effect is the formation zone concept. This is the distance from the production point which is required for the secondary hadrons to be formed and be able to interact as physical hadronic states. An advantage of neutrino induced interactions with respect to hadronic processes is the fact that the projectile interacts only once;

– In the correlated nucleon/quark models the backward particles are produced in the collisions off structures with mass larger than the mass of the nucleon. These structures are formed under the action of the short range component of the nuclear force, they represent the effects of gathering two or more nucleons in small volumes.

The full NOMAD sample of ν_μ CC events having a muon momentum of at least 3 GeV/c used in this analysis amounted to 944 000 events [79]. Only tracks attached to the primary vertex and having at least 8 DC hits were used in the search for backward particles. The separation between backward protons and pions was done on plots showing length vs. momentum. Protons were only visible in the plot of positive tracks having a relatively small length. With the help of MC simulations corrections were applied for reconstruction, stopping and identification efficiencies. The contamination of pions in the sample of identified protons amounted to 8 10^{-2} above 250 MeV/c.

The average number of backward proton per event was found to be around 510^{-2}. The rate was studied as a function of the hadronic energy E_{had} and of Q^2. A decrease of the yield with increasing E_{had} and Q^2 was observed. The slope parameter B of the invariant cross section, parameterized as $\exp(-Bp^2)$, has been measured and found to be consistent with previous ν-nucleus and hadron–nucleus experiments. Its value was: $B \sim 10\ c^2/\mathrm{GeV}^2$. This was in agreement with nuclear scaling previously observed in hadronic experiments. B was found not to depend on E_{had} and Q^2 over a wide range of values.

The backward proton rate measured in the NOMAD target (mainly carbon) has been compared with the values obtained on different nuclei. While the A dependence for neutrino scattering on heavy nuclei is consistent with that of hadron experiments, and can be parameterized as A^{α} with $\alpha = 0.68$, the NOMAD result does not fit this dependence. The A dependence of backward pions was found to be steeper than that of backward protons. The observed energy dependence was consistent with the formation zone mechanism. The correlation between the multiplicity of slow tracks and backward protons indicated the effects of reinteractions.

5.18. The importance of nuclear effects

We have just seen some complications coming from nuclear effects. Quarks and gluons are the basic degrees of freedom of hadronic matter. At high enough energy, neutrinos interact with quarks but quarks are not free, they are bound in the nucleons and because of confinement they are subject to Fermi motion. Moreover, at the level of the interaction, one has to take into account Pauli blocking, multinucleon effects and final state reinteractions. This brings a complication which is not entirely unraveled.

In particular this problem gives a challenge for oscillation measurements since it affects E_ν calculation. The beam energy is not known but must be reconstructed from the final state of the reaction. The accuracy of this reconstruction affects in particular the extraction of neutrino oscillation parameters. Nuclear effects bias the true E_ν; this is why it is important to understand nuclear effects.

The discrepancies noted in the experimental data concerning the measurement of the axial–vector form factor is a first hint that nuclear effects must be included in analyses of the data. It is now recognized that nucleon–nucleon correlations and two-body exchange currents must be added in order to provide a more accurate description of the ν-nucleus QE scattering. In particular, the multinucleon process called 2p–2h where the interaction happens on a dinucleon has to be taken into account. These effects yield enhanced cross sections at low neutrino energies [80,81]. They also produce final states that include multiple nucleons. Hence one needs to be careful in defining a QE event.

Another hint pointing to possible complications coming from nuclear effects comes with the long-standing anomaly of the LSND experiment. The detector made of 150 tons of liquid scintillator was exposed to a low energy (30 MeV) intense $\bar{\nu_\mu}$ beam at the Los Alamos beam-stop in the years 1993–1998. It found $88 \pm 22 \pm 6$ events compatible with interactions of $\bar{\nu_e}$. This "evidence" of oscillations was measured at the level of $2\ 10^{-3}$. It was never confirmed, on the contrary several subsequent experiments rejected the hypothesis. Recently nuclear effects were invoked to explain the signal. The MiniBooNE experiment was built to solve the problem, unfortunately, it observed "unexplained electron-like events in the reconstructed neutrino energy range from 200 to 475 MeV". The multinucleon emission channel included in the QE channel was suggested as a possible explanation of both effects.

Furthermore, CC QE total cross section on carbon is observed to be too large with respect to the theoretical predictions employing the standard value of the axial mass [82]. To explain this fact, it was suggested to consider events involving a correlated nucleon pair ejection. The inclusion in the QE cross section of events in which several nucleons are ejected, called np–nh excitations in the nuclear physics language, leads to an increased value over the genuine QE value. This could account for the excess in cross section without modifying the axial mass. The role that additional nuclear effects may play in neutrino–nucleus QE scattering remains the subject of much theoretical and experimental effort. There is no complete model yet.

The use of nuclear targets as detectors entails non-trivial problems as the interpretation of the observed signal requires quantitative understanding of the ν-nucleus interaction. With the present experimental accuracy, the treatment of nuclear effects is regarded as one of the main sources of systematic uncertainty.

Further investigation of neutrino interactions with nuclei is interesting from a nuclear many-body theory point of view. The parton description of Feynman is well verified by experiments, and the treatment described above takes for granted that one can neglect the action of strong interactions during the collision time. The fact that scaling laws are approximately obeyed in the real world is a non-trivial information on strong interaction dynamics, it leads to asymptotic freedom, but scaling cannot be exact since freedom sets in only asymptotically.

Analysis of data from the complete MINERνA experiment [83] will soon enable the first detailed look at nuclear effects in neutrino interactions. High statistics measurements of neutrino and antineutrino DIS are expected. The novelty of the experiment is to use systematically multiple nuclear targets of various compositions. It should be able to achieve a first detailed examination of such nuclear effects.

5.19. The MINERνA experiment at Fermilab

The MINERνA experiment (Main INjector ExpeRiment for ν A) is a neutrino scattering experiment which uses the o*n*-axis NuMI beamline at Fermilab. It is the most intense high-energy neutrino beam in the world, and thus it allows MINERνA

to use a relatively small detector with many sensitive channels per unit volume to zoom in on the details of the neutrino interaction. This attention to detail will allow MINERνA to study the properties of the nuclei struck by the neutrinos and also to examine neutrino reactions. It seeks to measure low energy neutrino interactions both in support of neutrino oscillation experiments and also to analyze the strong dynamics of the nucleon and nucleus that affect these interactions. It will do various complementary measurements with ν and $\bar{\nu}$ beams and different nuclei C, Fe, Pb.

The first detector module was completed in early 2006 and the first events were observed in 2009. Construction was completed and the detector installed in March 2010. Interactions of few GeV beams were studied until April 2012.

The full detector weighs 5 tons and is made of many layers of parallel scintillator strips. It is composed of a 3 m long active tracker followed by sampling EM and hadronic calorimeters. The tracker is based on a finely-segmented scintillator medium. The upstream portion of the detector includes planes of graphite, iron and lead interleaved between tracking planes to facilitate the study of nuclear effects in neutrino interactions. To identify particles emerging from the interactions, the MINERνA detector uses plastic scintillators . Each strip is connected to a photomultiplier tube which is used to detect the amount of energy deposited into the strip. The orientation of the strips varies from layer to layer so that three-dimensional information about where incoming particles interacted with the strip can be determined.

In fact the detector is installed in front of the MINOS (Main Injector Neutrino Oscillation Search) near detector which can be used as muon spectrometer. MINERνA has the goal of providing precision results which will have important impact on oscillation experiments. Initial data runs for muon neutrino and antineutrino beams of $\sim$3.5 GeV have produced a large number of new results for QE, pion production, and inclusive cross sections. First results have already shown evidence for the effect of multinucleon processes in elastic scattering.

Two different nuclear-medium effects are isolated using a low subsample of neutrino–carbon scattering data. The observed hadronic energy in CC ν_μ interactions is combined with muon kinematics to permit separation of the QE and $\Delta(1232)$ resonance processes. A small cross section is observed at very low energy transfer that matches the expected screening effect of long-range nucleon correlations. But additions to the event rate in the kinematic region between the QE and Δ resonance processes are needed to describe the data. In this kinematic region there is also an enhanced population of multi-proton final states. Contributions predicted for scattering from a nucleon pair have these properties; the model tested in the analysis is a significant improvement but does not fully describe the data. The 2p–2h model seems insufficient to explain the data. An improved description of the effects of the nuclear environment are required by current and future neutrino oscillation experiments.

A new high energy neutrino beam begun in summer 2013. Higher energies and rates will allow to measure with neutrinos the analog of the "EMC effect", found long ago with muon beams. This should shed more light on the dynamics of this nuclear modification of nucleon properties.

5.20. The liquid argon technique

A very promising new detection technique has been developed for many years: the use of noble liquids in a time projection chamber (TPC) type of apparatus. The preferred liquid is argon.

This new technique offers several advantages. The density of argon is rather large 1.4 g/cm^3, increasing the mass for a given volume and with the TPC technique it displays tracks with resolutions similar to the ones obtained with bubble chambers or NOMAD.

The first experiment to use this technique was ICARUS, a 600-tons detector which looked for high energy neutrino interactions coming from CERN under the Gran Sasso tunnel, 730 km away from the production source, in parallel with the OPERA detector.

Very recently a new experiment MicroBooNE [84] started to take data in a new short-baseline search at Fermilab. Neutrino energies in this beam are below 800 MeV. The experiment is designed to search for sterile neutrinos in order to confirm or refute the long-standing anomaly reported by the LSND collaboration and resolve the origin of a low energy excess of e-like events seen by MiniBooNE which took data in the same neutrino beam line.

MicroBooNE uses a 10.4 m long liquid argon TPC filled with 170 tons of liquid argon. In the argon, charged tracks ionize the medium and an electric field drifts the liberated electrons to a sensitive plane. The drift time reconstructs the depth coordinate, while the other two coordinates are measured in a X–Y array of crossed sense wires. The TPC reconstructs particle tracks as finely detailed 3-dimensions images. To do so, it is equipped with more than 8000 gold-plated wires set in three layers to capture pictures of interactions at different points in space and time. An array of 32 PMT's is used for triggering.

Fig. 25 shows one of the first neutrino events recorded by MicroBooNE. In the future it is foreseen to build a huge 20 ktons liquid argon TPC called DUNE to investigate long baseline neutrino oscillations at a distance of 1300 km from their production source situated at Fermilab.

5.21. Neutrinos at extreme energies

Neutrinos produced at accelerators reach an energy of up to $\sim$500 GeV. But there are sources of neutrinos of much higher energies originating in either atmospheric collisions of very high energy cosmic rays or directly from astrophysics processes. The neutrino cross-sections in this extreme energy range are essentially extensions of the high energy parton model. However, at these energies, the propagation term from interaction vertex is no longer dominated by the W–Z boson

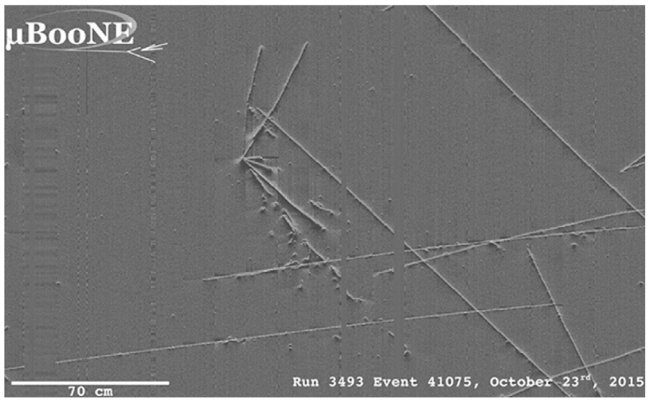

Fig. 25. A neutrino event recorded by the MicroBooNE detector.

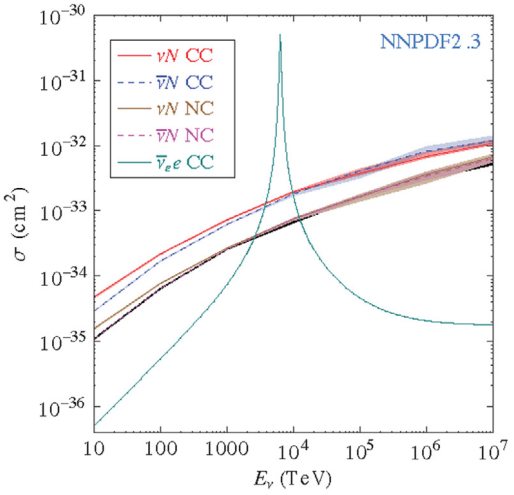

Fig. 26. Neutrino cross sections in the ultimate high energy regime.

mass. As a result, the cross-section no longer grows linearly with neutrino energy. In effect, the propagator term suppresses the cross-sections for energies above 10 TeV. Likewise the $(1-y)^2$ suppression that allows distinction between neutrinos and antineutrinos is less pronounced making the two cross sections closer. It is calculated that the neutrino cross sections at these high energies, 10^{16}–10^{21} eV follow a power law dependence [85] according to:

$$\sigma_\nu^{CC} = 5.510^{-36} E\,(\mathrm{GeV})^\alpha\ \mathrm{cm}^2$$
$$\sigma_\nu^{NC} = 2.310^{-36} E\,(\mathrm{GeV})^\alpha\ \mathrm{cm}^2$$

with the coefficient $\alpha = 0.36$.

There is one peculiar oddity. Neutrino–electron scattering is usually sub-dominant to any neutrino–nucleus interaction because of the small target mass. However there is one notable exception: when the neutrino undergoes a resonant enhancement from the formation of an intermediate W in $\bar{\nu}_e e^-$ interactions. This resonance formation takes place at $E_{res} = 6.3$ PeV and is by far more prominent than any νN interaction cross section. This mechanism was first suggested by Glashow [86] as a means to directly detect the W boson. When compared to that of neutrino–nucleon scattering , the $\bar{\nu}_e$ scattering dominates. Such high cross-sections can often cause the Earth to be opaque to neutrinos in certain energy regimes.

Fig. 26 shows these cross sections in the ultimate energy regimes above 10^4 GeV for CC and NC channels on nucleons and electrons including the Glashow resonance.

Direct neutrino scattering measurements at such extreme energies are unavailable. Predictions rely on existing knowledge of parton distribution functions but extrapolations in a domain of extremely small x result in substantial uncertainties. Already, observational programs have been developed. The most advanced techniques include detectors able to see interactions in large volumes of water like Antares [87] in the Mediterranean sea or ice like Amanda [88] and IceCube [89] in

the South Pole. Interactions are detected through the deposited light in optical modules. For the future, research is developing along other detection possibilities such as radiowaves. This is implemented in prototypes like Rice [90] or Anita [91].

We will take as an example the IceCube experiment which has already given evidence for extragalactic neutrinos.

5.22. The IceCube detector

Atmospheric and astrophysics neutrinos can reach enormous energies but their flux decreases very fast with energies. SuperKamiokande was able to measure atmospheric neutrinos with energies up to a few GeV. To catch higher energies it is necessary to use a much bigger detector and the only way is to instrument a naturally transparent medium either water or ice.

The IceCube Neutrino Observatory (or simply IceCube) is a neutrino telescope constructed at the Amundsen–Scott South Pole Station in Antarctica. It is the world's largest neutrino detector, its 5160 sensors are distributed over a cubic kilometer of volume under the Antarctic ice. Similar to its predecessor, the Antarctic Muon And Neutrino Detector Array (AMANDA), IceCube consists of spherical optical sensors called Digital Optical Modules (DOM's) which are distributed inside the ice, along strings lowered in vertical holes melted in the ice using a hot water drill, at depths ranging from 1450 to 2450 m. Each DOM has a photomultiplier tube and a single board data acquisition computer which sends digital data to the counting house on the surface above the array. The complete DOM's are deployed on 86 "strings" of sixty modules each, set 125 m apart.

IceCube device started to take data in December 2010. It is designed to look for point sources of neutrinos in the TeV range to explore the highest-energy astrophysical processes. It searches for neutrinos produced in the most violent astrophysical sources, for example events like exploding stars, gamma-ray bursts, and cataclysmic phenomena involving black holes and neutron stars. The IceCube telescope is a powerful tool to search for dark matter and could reveal the physical processes associated with the enigmatic origin of the highest energy particles in nature. In addition, exploring the background of neutrinos of atmospheric origin, IceCube studies the neutrinos themselves, their energies far exceeding those produced by accelerator beams.

When they interact with the molecules of the ice, neutrinos can create charged leptons (electrons, muons, or taus). These charged leptons can, if they are energetic enough, emit Cherenkov radiation. This happens when the charged particle travels through the ice faster than the speed of light in the ice, similar to the bow shock of a boat traveling faster than the waves it crosses. This light can then be detected by photomultiplier tubes within the DOM's. SuperKamiokande was already using the Cerenkov light produced in water to measure solar neutrinos.

The signals from the PMT's are digitized and then sent to the surface of the glacier on a cable. These signals can reconstruct kinematical parameters of the incoming neutrino. High-energy neutrinos may leave a large signal in the detector, pointing back to their origin. Clusters of such neutrino directions would indicate point sources of neutrinos.

Each of the above steps requires a certain minimum energy, and thus IceCube is sensitive only to very high energy neutrinos, in the range of 10^{11} to about 10^{21} eV. Estimates predict a neutrino event about every 20 min in the fully constructed IceCube detector originating from the atmosphere.

Of the different neutrino flavors, IceCube is most sensitive to muon neutrinos because muons are the most penetrating charged leptons and they leave the longest tracks in the detector. An electron resulting from a ν_e event scatters several times before losing enough energy to fall below the Cerenkov threshold; this means that ν_e events cannot be used to point back to sources, but they are more likely to be fully contained in the detector. These events are more spherical, or "cascade"-like, than "track"-like as are the ones originating from ν_μ events.

τ's can also create cascade events, but they are short-lived and cannot travel very far before decaying. They are usually indistinguishable from electron cascades. A τ could be distinguished from an electron with a "double bang" signature, where a cascade is seen both at the τ creation and at its decay. This is only possible with extremely high energy τ's. Hypothetically, to resolve a tau track, the τ would need to travel at least from one DOM to an adjacent DOM before decaying. Realistically, such double bang searches are centered at PeV scale energies. Analysis are under way but have not so far isolated such events.

However, there is a large background of muons created not by neutrinos from astrophysical sources but by cosmic rays impacting the atmosphere from above. There are about 10^6 times more cosmic ray muons than neutrino-induced muons observed in IceCube. A large part of these can be rejected using the fact that they are traveling downwards. Most of the remaining up-going events are from atmospheric neutrinos created from cosmic rays hitting the far side of the Earth.

About 75 upgoing neutrinos are reconstructed per day in the IceCube detector. Recent data show 54 events observed above 100 TeV with 20 ± 6 expected from the atmosphere. Three of them are above 1000 TeV giving a 7σ evidence for extraterrestrial neutrinos. Their distribution is largely isotropic confirming the extragalactic origin. These neutrinos are the key to IceCube point source searches.

In fact the discovery came in 2012, when IceCube reported the observation of two ultra-high-energy neutrino events. They were in the PeV energy range, making them the highest energy neutrinos to date. The pair were nicknamed "Bert" and "Ernie", after characters from the Sesame Street TV show. An even more energetic neutrino was discovered in 2013 and given the name "Big Bird". This opens the way to detect astrophysical neutrinos and the search is going on. The arrival directions of these astrophysical neutrinos are the points with which the IceCube telescope maps the sky.

In the other hemisphere the Antares detector has been taking data in the Mediterranean sea. Although having a smaller size, its position complements that of IceCube since it is able to explore the other half of the sky. Analysis are under way and Antares already excludes a point source at our galactic center.

As a development of these efforts, both collaborations are building denser arrays in the heart of the existing ones. The aim is to lower the threshold of ν observations to a few GeV. PINGU will be built inside the IceCube apparatus and ORCA inside Antares. These new detectors could resolve the problem of the neutrino mass hierarchy found in oscillations by studying atmospheric neutrinos crossing various amount of matter when traversing the Earth.

6. Matter effect and neutrino oscillations

We have discussed in details many different neutrino interaction channels, both on electrons, nucleons or quarks. But neutrinos can also interact with matter "as a whole". This is a process which arises when neutrinos cross matter, although it does not result in a proper interaction with the creation of secondary particles. It is a very important aspect of the behavior of neutrinos since it permits to fix fundamental parameters, namely masses and mixings among neutrino flavors. This is realized through the phenomenon of neutrino oscillations, namely the spontaneous change between different types of neutrinos. This is now proven experimentally.

Simple oscillations arise in vacuum because of different masses characterizing the different flavors, but oscillations can also take place even in the case of massless neutrinos if the propagation occurs in matter. This arises because matter is not "leptonicly neutral" for neutrinos. Matter contains electrons, it does not contain muons or taus, thus different neutrino flavors feel matter differently. In order to understand this new type of phenomenon, let us shortly describe how oscillations come about.

6.1. What are neutrino oscillations?

Up to the years 1980 the main interest in neutrino physics was limited to the study of weak interactions, neutrinos were a tool to understand the weak structure of matter. But then a problem of cosmological importance came up and the question of the neutrino masses became crucial. Direct limits on masses of the three active neutrinos existed but these limits were not very constraining, and it appeared that the most powerful way to fix neutrino masses was to study their oscillations, when they spontaneously change from one type to another. Notice that this is a revolutionary proposal in the sense that it violates leptonic charge conservation introduced at the beginning and which was considered as a sacred rule.

The three active neutrinos ν_e, ν_μ and ν_τ have a well-defined leptonic number, they are called weak interaction eigenstates. They are operative both when they are produced and when they interact through weak processes, namely at the birth and death of the particle. But a different set of states has to be introduced at the level of their propagation in time or space. The effective states relevant during a time evolution, dictated by the Schrödinger equation, are the ones corresponding to a well-defined energy or mass. For three active weak neutrinos, one must introduce three mass eigenstates usually called ν_1, ν_2 and ν_3.

For the simple case involving only two flavors, a mixing matrix relates the weak states ν_e, ν_μ and the mass states ν_1, ν_2. It is a unitary 2×2 matrix introducing a new parameter, a mixing angle θ, very similar to the Cabibbo angle appearing among quarks:

$$\nu_e = \nu_1 \cos\theta + \nu_2 \sin\theta$$
$$\nu_\mu = -\nu_1 \sin\theta + \nu_2 \cos\theta.$$

Having different masses ν_1 and ν_2 evolve differently in time, they develop a phase shift during their propagation. After some time, a pure flux of ν_e (or ν_μ) changes into a mixture containing some ν_μ (or ν_e). This process is called oscillation and it is quantified by a probability which depends on the length over which it develops. Over a distance L, it is given by the formula:

$$P = \sin^2 2\theta \sin^2 2(\pi L/\lambda).$$

In this formula, λ is the so-called oscillation length which is given by the formula:

$$\lambda\,(\mathrm{km}) = 2.5E\,(\mathrm{GeV})/\delta m^2\,(\mathrm{eV}^2)$$

where E is the energy of the neutrino in GeV and δm^2 is the difference between the squared masses of ν_1 and ν_2 in eV^2. In practice, the amplitude of the oscillation is driven by the term $\sin^2 2\theta$ while its frequency is driven by δm^2. Note that the parameter $\sin^2 2\theta$ is often referred as U^2_{e1}, U being the unitary matrix relating the two sets of neutrino states. The phenomenon is similar to the precession of a spin evolving in a magnetic field. It is a direct consequence of the Heisenberg uncertainty principle applied to the neutrinos, because the phenomenon violates the conservation of energy or momentum at the moment of the change.

Examining the dimensions which appear in the formula, it is evident that this phenomenon can probe neutrino masses in the eV/c^2 range and below. For example for a 1 eV/c^2 scale, the oscillation develops over a few meters in the case of reactor neutrinos (MeV energies) and over a few kilometers for accelerator neutrinos (GeV energies). This allows very precise experimental measurements. There is a limitation: although an oscillation experiment tests very small masses, it only gives information on a difference of masses. The absolute values of neutrino masses will have to be fixed by complementary informations.

As we know, there exist not two but three types of neutrino flavors and a straightforward generalization can be done. With ν_e, ν_μ and ν_τ, one must introduce three mass-eigenstates ν_1, ν_2 and ν_3, which propagate independently in space. The unitary mixing matrix relating the weak and the mass eigenstates is now of dimension 3×3; it is similar to the CKM (Cabibbo–Kobayashi–Maskawa) matrix relating quarks. It is called the PMNS matrix (for Pontecorvo–Maki–Nakagawa–Sakata). This matrix has 9 elements. It can be parameterized with three different mixing angles, θ_{12}, θ_{13}, θ_{23}, but, like the CKM matrix, it also involves a supplementary phase usually called δ which could be at the origin of CP violation in the lepton sector. In the case of Majorana neutrinos, two different phases need to be introduced.

Experimentally, there are two complementary ways to probe the phenomenon of oscillations:

– the disappearance method, where the original neutrino flavor produced at a given source is diminished with respect to the calculated one obtained in the case of the no-oscillation hypothesis.

– the appearance method, where a new flavor is detected which is absent in the original flux.

The appearance method is more powerful since a few well-identified events are enough to prove the phenomenon. On the contrary, the disappearance measurement relies on the difference between two numbers, the one of expected events and the one of detected events.

Experimentally, the first hint of oscillations came from the disappearance of solar neutrinos of type ν_e, the apparent deficit already discussed. This deficit was seen with the Chlorine experiment, then by Gallex, SuperKamiokande and finally SNO. It was confirmed by a deficit of reactor neutrinos measured with the KamLAND detector counting fewer interactions than expected from Japanese reactors situated at an averaged distance of 180 km. Atmospheric neutrinos also showed a deficit when analyzing the flux of ν_μ crossing the diameter of the Earth. This was clearly measured by the SuperKamiokande experiment and later it was confirmed by the MINOS detector at Fermilab, then by the OPERA one.

Oscillation phenomena only depend on mass differences. The various oscillation channels, within the framework of 3 neutrinos, involve two independent mass terms, for example δm_{12} and δm_{23}, the third combination δm_{13} being directly correlated to the first two. The absolute masses cannot be determined by oscillations. Of course, oscillation experiments provide a lower bound on the heavier mass but upper bounds must come from other considerations.

Present results give:

– from observations of solar and reactor neutrinos: $\delta m^2_{12} = (7.49 \pm 0.19)\ 10^{-5}\ \mathrm{eV}^2/c^4$.

– from atmospheric and accelerator neutrinos: $\delta m^2_{23} = (2.50 \pm 0.10)\ 10^{-3}\ \mathrm{eV}^2/c^4$.

In the simplest scenario of no-degeneration between the masses, and assuming a normal mass hierarchy ($m_3 \gg m_2 \gg m_1$), this would give the three individual masses:

$m_3 \sim 50\ \mathrm{meV}/c^2$, $m_2 \sim 8.5\ \mathrm{meV}/c^2$, with m_1 much smaller than the other two.

Note that, although these masses are extremely small, cosmological neutrinos which decoupled 1 s after the Big Bang are predicted to be so numerous, about $300/\mathrm{cm}^3$ through all the space, that the total mass of the existing neutrinos is about the same as the total mass of all the stars present in the Universe.

6.2. The Wolfenstein effect

Neutrinos undergo refraction while moving in a medium. It is a coherent effect of propagation through matter. A plane wave propagating in an homogeneous medium has the space dependence:

$$\Psi(x, t) = e^{p.x} e^{-iEt}.$$

If the incident wave propagates in matter, a second scattered wave adds up. When the diffusion is small, absorption of the incident wave is negligible but the forward amplitude is slightly modified. This effect can be described by a refraction index n. The total wave becomes:

$$\Psi_{tot}(x, t) = e^{np.x} e^{-iEt}$$

with $n = 1 + 2\pi \rho_N f(0)/p^2$

ρ_N is the atomic density and $f(0)$ the forward scattering amplitude. One can calculate that $(n - 1)$ is of the order of $6\ 10^{-19} \rho_N \mathrm{Z/A}$ for neutrinos of energy 1 MeV.

If n were the same for all flavors of neutrinos, the same supplementary phase would develop for all types and the oscillation which depends on a difference of phases would remain unchanged. But, as was said before, ordinary matter contains electrons with which ν_e have elastic scattering amplitudes different from the other flavors because of W-exchange. A different phase-shift develops between flavors. This was recognized as early as 1978 [92].

This has a direct consequence: oscillations occur in matter with amplitude (or mixing angle) and length which are different from their values in the vacuum. In the simple case of only 2 neutrino flavors, ν_e and ν_μ, the oscillation inside matter having a constant density, develops according to new parameters θ_m and $Ł_m$ different from the vacuum values θ_v and $Ł_v$ coming from the mass effects alone. The new parameters are given by:

$$\sin^2(2\theta_m) = \frac{1}{1 + (R-1)^2 \cot g^2 2\theta_v}$$

$$Ł_m = \frac{Ł_v}{\sin 2\theta_v \sqrt{(1 + (R-1)^2 \cot g^2 2\theta_v)}}.$$

The parameter R is given by $R = \rho_e/\rho_R$ where ρ_R measures the phase shift between ν_e and ν_μ:

$$\rho_R = \frac{(E_2 - E_1)\cos 2\theta_v}{\sqrt{2}G}.$$

Even if mixing angles in vacuum are small, large oscillation amplitudes can develop in matter. In particular a resonance effect can take place as we discuss now.

6.3. The MSW resonant mechanism

As we have seen, neutrino oscillations are affected by the presence of matter with the possible resonant amplification of the process as originally discussed by Mikheyev and Smirnov [93].

The interesting fact is that, in the formulae given above, the oscillation probability exhibits a resonance behavior. It becomes maximum when $R = 1$, that is if $\rho_e = \rho_R$. The mixing angle in matter $\sin^2(2\theta_m)$ reaches unity, the oscillation is maximum no matter how small is θ_v. There is a complete disappearance of the original flavor with an oscillation length corresponding to $L_R = L_v/\sin 2\theta_v$.

For a given medium, the resonance depends on the energy. For example in the case of the Earth, assuming a constant density $\rho_e \sim 1.5 N_A e/\text{cm}^3$, the resonant energy is 5 $\delta m^2(\text{eV}^2)\cos 2\theta_v$ TeV and the resonant oscillation length is $12500/tg2\theta_v$ km. This is a distance that is larger than the Earth diameter.

We discussed the deficit of solar neutrinos: various experiments probing various neutrino energy ranges measured between 0.3 and 0.4 of the predicted flux. Can matter effect explain this?

At the center of the Sun, where the neutrinos are produced, the density is $\rho_c = 150$ g/cm^3 with a nuclear ratio Z/A of 2/3. The electronic density decreases more or less exponentially from the center to the edge following the variation:

$\rho_e = \rho_c \exp(-R/R_0)$ with $R_0 = 70000$ km and $\rho_c = 6\ 10^{25} e^-/\text{cm}^3$.

Near the edge the density is much reduced and reaches $10^{-4}\rho_c$. The critical density at which the resonance occurs vary with energy, but this critical density will be crossed at a certain point of their travel by the neutrinos escaping the Sun, no matter their initial energy. As a consequence, the resonant condition is fulfilled in the interior of the Sun, and this explains the solar deficit which remained a puzzle for a long time because initially physicists privileged an oscillation between the Sun and the Earth. This possible interpretation gave inconsistencies and now the MSW process is fully accepted.

This has a direct consequence. We discussed the unknown mass hierarchy between the three neutrinos. Matter effects in the Sun fixes the hierarchy between ν_1 and ν_2: ν_1 is lighter. This restricts the uncertainty between the three masses to a two-fold ambiguity, and one has today the two possibilities of either the normal mass hierarchy (NH), $m_1 \leq m_2 \leq m_3$ or the inverted mass hierarchy (IH), $m_3 \leq m_1 \leq m_2$. This ambiguity remains one of the pending problems in neutrino oscillations to resolve in priority.

6.4. The NOνA detector

Oscillations in vacuum depend on a difference of squared masses between the two mass eigenstates involved. In order to extract an absolute scale between the three masses, another information must be obtained. This explains why the situation in oscillation measurements has two possible solutions as was just discussed above: NH or IH.

We know that m_1 is smaller than m_2 because of solar neutrino oscillations, this is explained by matter effects inside the Sun. In order to assign the order of the third mass, another matter effect has to be put to a test. This is the reason of a new experiment set up in an accelerator beam and positioned far from the neutrino source.

This is again a long-baseline experiment to search for ν_μ disappearance and ν_e appearance in a ν_μ beam. Several examples were built in the past to confirm oscillations, in particular MINOS and OPERA already presented. The emphasis is now on measuring matter effects to discriminate between the NH or IH solutions, and this particular task requires some special adjustments.

We describe in some details the NOνA experiment which starts taking data in a neutrino beam originating from the Fermilab accelerator and which is positioned at a distance of 810 km from the source in Ash River, Minnesota.

NOνA is a 14 kilotons totally active scintillator detector made of liquid scintillator [94]. It is positioned, not on the axis of the beam but 0.8 degrees off-axis. This position reduces drastically the neutrino flux, but has the crucial advantage of giving a sharp energy peaked around 2 GeV, close to the first oscillation maximum set at 1.7 GeV by previous search experiments in the $\nu_\mu \rightarrow \nu_e$ channel. This represents a modern version of the old use of narrow band beams.

During a first period of data taking, 6 10^{20} protons were sent on target. Simulations have been done with a constant Earth mass density of 2.8 g/ cm^3; at this level of accuracy the variations and uncertainties of the crust details can be neglected. The other entering parameters like difference of masses and mixing angles are taken from the best previous measurements.

Matter effect enhances the separation between the oscillation spectra and therefore the event rates in the case of NH or IH. NH enhances ν_e appearance in the ν_μ beam while IH enhances $\bar{\nu_e}$ appearance in the $\bar{\nu_\mu}$ beam. Only two possibilities exist and the "discovery" of the mass hierarchy is defined as the ability to exclude degenerate solutions for the wrong hierarchy at a given confidence level. Notice that the other unknown parameter in neutrino oscillations the CP phase angle δ_{CP} has to be disentangled. It is essential to take advantage of all the observations to extract a consistent interpretation of various available data obtained with both neutrino and antineutrino beams to resolve degeneracies, from NOνA but also from the Japanese

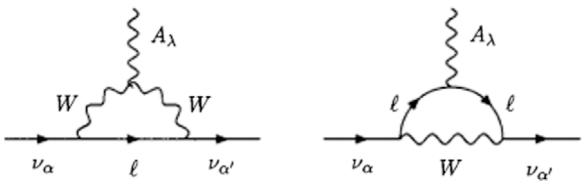

Fig. 27. Feynman diagrams for the coupling between neutrinos and photons.

T2K experiment which runs at smaller energy with a baseline of 295 km using SuperKamiokande as far-away detector. The final answer is not yet known but present analysis seem to suggest NH.

One does not expect to resolve completely the whole puzzle with the present generation of experiments. Unraveling neutrino mass hierarchy, CP-violation and also the octant of θ_{23} which is still unknown is a difficult endeavor. Present experiments can provide a hint only for favorable ranges of parameters at limited confidence level. Hence new long-baseline experiments with longer path, more intense beam sources and advanced techniques are already programmed in particular the DUNE project which will rely on a huge liquid argon detector positioned in a deep mine at the Sanford Underground Laboratory in South Dakota, 1300 km away from the Fermilab neutrino source. It will be a huge liquid argon detector of 20 ktons to be operational in 2024.

6.5. Coherent scattering on nuclei

A new possibility of neutrino interaction is predicted by the Standard Model, the possibility of coherent neutrino scattering on nuclei. Shortly after the discovery of NC neutrino reactions, it was pointed out that the neutrino–nucleus interactions should also exist [95], and this could be very advantageous at low energies, the cross section becoming coherent across all the nucleons present in the nucleus. As a result the cross section could grow drastically. Such an enhancement is possible if the momentum transfer of the reaction is much smaller than the inverse of the target size. To achieve a coherent scattering, the neutrino wave length must be larger than the size of the nucleus, neutrinos of less than 10 MeV offer this possibility.

The calculation gives the following cross section:

$$\frac{d\sigma_C}{d\cos\theta} = \frac{G^2}{8\pi} E_\nu^2 (1+\cos\theta)[Z(4\sin^2\theta_W - 1) + N]^2$$

where Z and N are the numbers of protons and neutrons present in the target. The amplification can be huge in the case of heavy nuclei. In fact it goes approximately as N^2. Unfortunately the experimental signature is extremely feeble. The maximum recoil energy given to the nucleus is limited by the kinematics of the elastic collision:

$$T_{max} = \frac{E_\nu}{1 + M_A/(2E_\nu)}.$$

In principle, the conditions can be met at a reactor. Calculations predict about 10 events per day in a Na target of 1 kg with a maximum recoil energy of 0.8 keV. To detect such small signal, the only possible technique to be envisaged is the use of cryogenic detectors. Bolometers could be sensitive enough to measure the heating and the ionization due to such energy recoils, but bolometers are still very limited in size.

Despite the strong coherent enhancement enjoyed by this process, this particular interaction has yet to be detected experimentally. Many attempts have been proposed in the past using various techniques, without success. The experimental problem is to suppress the background coming from ambient radioactivity, and new attempts are being developed.

7. Electromagnetic interactions of neutrinos

Let us now discuss a new type of interactions of neutrinos with matter which can in principle be envisaged. Although electrically neutral, neutrinos can participate in electromagnetic interactions by their coupling to photons via loop diagrams.

7.1. The coupling between neutrinos and photons

As a second order process, graphs exist which couple neutrinos and photons through a charged loop. This gives rise to magnetic moments and radiative decays. The diagrams are shown in Fig. 27.

This type of graph is GIM (Glashow–Iliopoulos–Maiani) suppressed and the corresponding processes are extremely reduced at least in vacuum. But the GIM suppression does not hold in a medium because of the presence of the electromagnetic nuclear field, and electromagnetic processes can be hugely amplified in matter. For example the radiative lifetime can be shortened by an enormous factor of 10^{24} in a crystal of germanium.

7.2. Magnetic moment of the neutrino

As for other particles the electromagnetic properties of the neutrino can be described by form factors. Four independent parameters have to be introduced for Dirac neutrinos: charge and axial charge form factors, and electric and magnetic dipole moment form factors. At $Q^2 \rightarrow 0$ the first two vanish and the latter two reach the values of the so-called electric and magnetic dipole moments. The electric dipole moment vanishes because of the CPT theorem. It remains the magnetic one.

Notice that a Majorana neutrino would have no charge radius, no magnetic moment and no electric dipole moment. This is a consequence of the CPT theorem which imposes that a particle and its antiparticle must have charges, magnetic moments... equal in magnitude and opposite in sign.

As soon as the Dirac neutrino has a mass, it gets a magnetic moment. The Standard Model predicts the minuscule value [96]:

$$\mu_\nu = 3.210^{-19}(m_\nu/\mathrm{eV})\mu_B$$

where μ_B is the Bohr magneton.

With the known values of neutrino masses, this is extremely small. But models exist which may give much increased values such that an experimental search can be useful in setting limits.

A magnetic moment would give an anomalous electromagnetic interaction resulting in a new contribution to the reaction:

$$\nu + e^- \rightarrow \nu + e^-.$$

The corresponding cross section is:

$$\frac{d\sigma}{dT} = \frac{G^2 m}{2\pi}\left[(g_V + x + g_A)^2 + (g_V + x - g_A)^2(1 - T/E_\nu)^2 + (g_A^2 - (x + g_V)^2)\frac{mT}{E_\nu^2}\right] + \frac{\pi\alpha^2\mu_\nu^2}{m^2}\frac{1 - T/E_\nu}{T}$$

T is the kinetic energy of the recoiling electron and x is related to the charged radius r_e: $x = 2m_W^2/3(r_e^2)\sin^2\theta_W$.

The process would give an isolated electron peaking at small energy, contrary to the electroweak contribution. The largest sensitivity to a magnetic moment is at very low T. Such events have been searched in elastic neutrino scattering on electron, for both ν_e and ν_μ beams at LAMPF, at CERN with the BEBC bubble chamber, and also at nuclear reactors.

The present best limits obtained so far with beams are:

$$\mu(\nu_e) \leq 10^{-9}\mu_B$$
$$\mu(\nu_\mu) \leq 10^{-10}\mu_B.$$

A dedicated experiment called MUNU was set-up at the Bugey reactor [97]. It consisted of a 1 m^3 large TPC loaded with CF_4 at 5 bar pressure. It was surrounded by a large active shielding of liquid scintillator spied by photomultiplier tubes augmented by a passive shielding of lead. It was possible to measure the emitted electron energy down to 500 keV and also its direction which is a crucial help in order to suppress background.

A very different set-up is being developed by the TEXONO-CDEX Collaboration (Taiwan EXperiment On NeutrinO-China Dark Matter EXperiment) [98]. The technology of high-purity germanium HPGe detection is explored to develop a sub-keV threshold detector. This would enable studies on low energy neutrinos and also dark matter physics. The generic benchmark goals in terms of detector performance are to obtain a modular target mass of order of 1 kg with a sensitivity reaching the range of 100 eV. The TEXONO program has already contributed to the study of neutrino magnetic moments with a 1-kg HPGe detector surrounded by scintillating NaI(Tl) and CsI(Tl) crystals as anti-Compton detectors. It was set-up at a distance of 28 m from the 2.9 GW reactor core of the Kuo-Sheng Nuclear Power Station in Taiwan. A detection threshold of 5 keV and a background level of 1 event/kg/keV/day at 12–60 keV were achieved. A limit on the neutrino magnetic moment was derived from these measurements. Based on 4712 and 1250 h of reactor ON and OFF data respectively, the limit obtained at 0.90 C.L. on the neutrino magnetic moment was:

$$\mu(\nu_e) \leq 1.310^{-9}\mu_B.$$

This novel detector technique is also adapted to explore the study of neutrino–nucleus coherent scattering which was discussed before.

This is still extremely far from the Standard Model expectation which predicts a magnetic moment at the level of order $10^{-19}\mu_B$ for a neutrino mass of 1 eV/c^2.

7.3. Radiative decays of the neutrino

Another physical process allowed by electromagnetic interactions of neutrinos is the radiative decay $\nu_H \rightarrow \nu + \gamma$ where ν_H has a mass m_2 higher than m_1 the one of ν. In the SM, this decay corresponds to the type of graph already shown in Fig. 27. The two simplest Feynman diagrams are shown. Of the two contributing graphs, the one attaching the photon to the lepton leg gives the strongest contribution because of the high W mass. The result is a detectable photon and this process was calculated long ago [99]. The result is not encouraging with a rate (in s^{-1}):

$$\Gamma \sim 10^{-44}(m_2/\mathrm{eV})^{-5}(1 - x^2)^3(1 + x^2)U_1^2U_2^2$$

with $x = m_2/m_1$ and $U_1^2U_2^2$ denoting two mixings appearing at the vertices of the graphs.

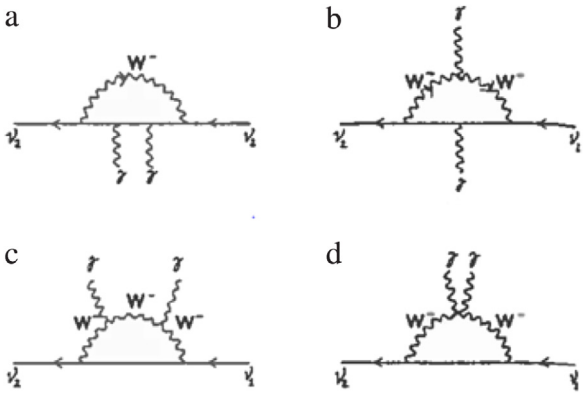

Fig. 28. Feynman diagrams for the two-photon decay of the neutrino.

The calculation gives an extremely long lifetime when the mass is below 1 MeV/c^2. A normal neutrino of 1 eV/c^2 mass would have a lifetime longer than $7\ 10^{43}$ s, that is about 10^{26} times the age of the Universe. Like other weak processes the lifetime varies as m^{-5}.

Radiative neutrino decays have been searched at reactors, looking for individual photons, at LAMPF using pion and muon decays at rest, from the X-ray emission of the Sun and from the explosion of SN1987A. In this latter case 10 $\bar{\nu}_e$ interactions were detected in Kamiokande and the same number in IMB with an energy of $\sim$ 20 MeV. The idea was to correlate these signals with a possible photon burst coming from the same direction in the sky. Photons from such neutrino decaying in flight from the supernova distant 150 000 light-years from us, would carry half of the neutrino energy. No excess of γ rays in the range of $\sim$10 MeV were found and a limit was set [100]:

$$\tau \geq 2.810^{15}(m_\nu/\text{eV})s.$$

The TEXONO experiment has given an indirect bound of the ν_e radiative lifetime of:

$$m_\nu^3\tau_\nu \geq 2.810^{18}\ \text{eV}^3\ \text{s}.$$

This is still very far from the theoretical expectations.

It is interesting to note that the enormously long lifetime applies in vacuum. It has been pointed out that the radiative decay is very efficiently amplified in matter [101]. It is still experimentally hopeless to test in the laboratory. Nevertheless among the possible decays, it is worth mentioning the two-photon mode which could be highly favored. This is another way to avoid GIM suppression. Although it is still out of reach for active neutrinos which masses are below 0.1 eV/c^2, this process is interesting when applied to neutrinos of higher masses. The process $\nu_H \rightarrow \nu + \gamma + \gamma$ can be calculated by the graphs of Fig. 28. It can largely dominate over the single photon radiative mode for some range of ν_H masses, depending on the relevant mixing angles. It may be important as a possible detection channel in the future. But contrary to the one photon decay, it gives a continuous spectrum much more difficult to identify than a mono-energetic ray.

Other decay modes exist. There is always the possibility of decays into three neutrinos, but this is useless from an experimental point of view. For a neutrino mass high enough, one can in principle consider the mode $\nu_H \rightarrow e^+e^-\nu_e$. But this is possible only if the mass of the decaying neutrino is above the $e^+e^-\nu_e$ threshold namely 1 MeV/c^2. With our present knowledge, this is now excluded for the three active neutrinos. But it remains an interesting signature to look for new heavier types of neutrinos, the so-called sterile neutrinos ν_H which have gained recently a lot of interest.

7.4. A puzzling hint

In effect, an intriguing indication was recently suggested with data from the XMM-Newton telescope [102]. It showed a narrow line in the X-ray spectrum of galaxy clusters. Two groups have reported an unidentified spectral line at the energy $\sim$3.5 keV in the stacked X-ray spectra of the Andromeda galaxy, Perseus galaxy clusters and the Galactic Center of the Milky Way. This is shown in Fig. 29.

This could originate from the radiative one-photon decay of a neutrino having a mass of 7 keV/c^2 and the proposed lifetime calculated from the hypothetical density under scrutiny is 10^{28} s.

We know from oscillation measurements and limits coming from CMB (Cosmic Microwave Background) that the masses of the three known neutrinos are much below this value. The present upper limit given by Planck and BAO is $\Sigma m \leq 0.16$ eV for the sum of the three masses. But theory allows the existence of a new kind of neutrinos potentially with higher masses, the sterile neutrinos already alluded to.

In fact, in the Standard Model the existence of right-handed neutrino fields is almost compulsory in order to understand the, although tiny, masses of the active neutrinos. These new neutrinos, if they exist do not undergo weak interactions, thus

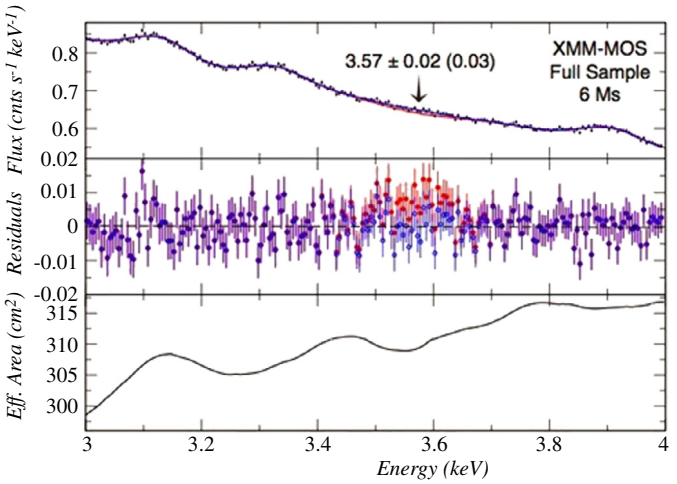

Fig. 29. Hint of a monoenergetic photon signal.

they are named sterile. They couple to the "real world" only through mixing with the known neutrinos. Their masses are completely unknown. In the original model of the see-saw mechanism [103], masses of singlet neutrino fields are extremely high, at the level of the scale of lepton number violation. But other models exist allowing masses as small as some keV/c^2 for the type associated to ν_e. Such a mass would allow radiative decays but with a lifetime much higher than the age of the Universe. The interesting point is that such neutrinos could indeed be good candidates to explain the Dark Matter of the Universe. Proponents of this explanation point out that calculations show better agreement with the measured profile of the missing mass obtained with such objects than the one obtained with heavy WIMP's. Born ultrarelativistically like radiation they behave as a^{-4} in the early Universe, but later they evolve as a^{-3} just as dark matter does. They give the so-called Warm Dark Matter solution to the missing mass problem.

This explains the interest in the result presented here. A 7 keV/c^2 sterile neutrino responsible for the Dark Matter would completely change our understanding of cosmology. It is being widely discussed in the literature. Existing data do not allow to completely exclude the possibility that this line may originate from an atomic transition. However the distribution of this signal over the sky and the ratios of its strength observed in different objects are consistent with predictions for decaying DM.

This result is obviously extremely important and measurements with higher precision are underway to confirm or disprove it. Unfortunately a first satellite launch, Astro-H failed, and we will have to wait longer for a definitive answer.

8. Conclusion

The main aim of this review was to give a full account of the many aspects of neutrino interactions with matter. The discussion has ranged from ∼100 keV to PeV energy scales spanning a broad range of physics processes, but excluding the case of cosmological neutrinos below the eV range where no practical ideas of possible detection have emerged yet.

Experimental data have supported the theoretical calculations, thus strengthening the foundations of the SM. Until recently a last piece of the construction was missing: the existence of the Higgs boson. This has been achieved and the mass of this last object, 125 GeV/c^2, has been found in the region predicted by the theory. This is a tremendous achievement. Nevertheless the situation is not satisfactory. There are some fundamental pending questions to be understood: the existence of Dark Matter and of Dark Energy, the disappearance of antimatter since the times of the Big Bang. Neutrinos could have the answer to some of the present puzzles: sterile neutrinos have been advocated as possible candidates for Dark Matter, neutrinos with varying masses could mimic Dark Energy, the δ phase of CP violation searched-for in neutrino oscillations could explain the asymmetry between matter and antimatter in the present Universe. These mighty questions should be addressed in the coming years. Intrinsic properties of the neutrinos have given the first hints of a more complete theory. The discovery of their masses, not embedded in the Minimum Standard Model, was the first sign that a more complete vision arises.

Still, a more basic question comes up. A final theory should explain everything with a minimum number of ingredients but the Standard Model is built on a large number of arbitrary parameters, masses, mixings, couplings, and on this front neutrinos have worsened the situation requiring 7 new parameters: three masses, three mixing angles and one (maybe two) CP phase. Some theorists claim that string theory is the answer towards a final theory, but it seems that string theory exceeds by far the experimental possibilities of verification, it lies beyond the frontiers of physics.

There is a list of problems to be solved and future will tell how far the human intelligence can progress and if the full knowledge of how the Universe works is within the reach of our comprehension.

I wish to thank J.M. Levy and B. Popov for their friendly help.

References

[1] C.L. Cowan, et al., Science 124 (1956) 528.
[2] G. Danby, et al., Phys. Rev. Lett. 9 (1962) 36.
[3] M. Perl, et al., Phys. Rev. Lett. 51 (1975) 1945.
[4] K.A. Olive, et al., Chin. Phys. C 38 (2014) 090001.
[5] F.J. Hasert, et al., Phys. Rev. B 46 (1973) 138.
[6] F.J. Hasert, et al., Phys. Rev. D 17 (1975) 768.
[7] S. Weinberg, Phys. Rev. Lett. 19 (1967) 1264.
[8] L. Maiani, in: K. Winter (Ed.), Neutrino Physics, Cambridge University Press, 1991, p. 278.
[9] J.A. Formaggio, G.P. Zeller, hep-ex 1305 7513 2013.
[10] R.P. Feynman, Photon-Hadron Interactions, Benjamin, 1972.
[11] A. Hoummada, et al., Appl. Radiat. Isot. 46 (1995) 449.
[12] G. Zacek, et al., Phys. Rev. D 34 (1986) 2621.
[13] B. Achtar, et al., Nuclear Phys. B 434 (1995) 503.
[14] G.S. Vidyakin, et al., J. Exp. Theor. Phys. 93 (1987) 424.
[15] M. Apollonio, et al., Eur. Phys. J. 27 (2003) 331.
[16] F. Boehm, et al., Phys. Rev. D 64 (2001) 11.
[17] A. Gando, et al., Phys. Rev. D 83 (2011) 5.
[18] J.I. Crespo-Anadon, arxiv:1412.3698v1, 2014.
[19] S.B. Kim, arxiv:1412.2199, 2014.
[20] F.P. An, et al., Phys. Rev. Lett. 112 (2014) 061801.
[21] F.P. An, et al. arxiv:1507.05613, 2015.
[22] G. Mention, et al., Phys. Rev. D 83 (2011) 073006.
[23] B. Zeitnitz, et al., Prog. Part. Nucl. Phys 32 (1994) 351.
[24] C. Athanassopoulos, et al., Phys. Rev. C 55 (1997) 2080.
[25] L.B. Auerbach, et al., Phys. Rev. D 63 (2002) 11.
[26] I.E. Lagaris, V.R. Pandharipande, Nuclear Phys. B 359 (1981) 331.
[27] M. Brack, C. Guet, H.-B. Hakansson, Phys. Rep. 123 (1985) 275.
[28] A.I. Abazov, et al., Phys. Rev. Lett. 67 (1991) 3332.
[29] P. Anselmann, et al., Phys. Rev. B 342 (1995) 440.
[30] K.S. Irata, et al., Phys. Rev. Lett. 63 (1989) 6.
[31] R. Bencker-Szendy, et al., Nucl. Instrum. Methods 324 (1993) 363.
[32] S. Fukuda, et al., Nucl. Instrum. Methods 501 (2003) 418.
[33] Q. Ahmad, et al., Phys. Rev. Lett. 97 (2001) 071301.
[34] F. Reines, et al., Phys. Rev. Lett. 37 (1976) 315.
[35] S. Riley, et al., Phys. Rev. C 59 (1999) 1780.
[36] B. Aharmin, et al., Phys. Rev. Lett. 101 (2008) 11130.
[37] P. Astier, et al., Nucl. Instrum. Methods 515 (2003) 3.
[38] K. Kodama, et al., Phys. Lett. B 504 (2001) 218.
[39] M. Tzanov, et al., Phys. Rev. D 74 (2006) 012008.
[40] Q. Wu, et al., Phys. Lett. B 660 (2008) 19.
[41] M. Adamson, et al., Phys. Rev. D 81 (2010) 0720029.
[42] M. Holder, et al., Phys. Rev. Lett. 39 (1977) 488.
[43] A.N. Diddens, et al., Nucl. Instrum. Methods 178 (1980) 27.
[44] J. Altegoer, et al., Nucl. Instrum. Methods 404 (1998) 96.
[45] M. Holder, et al., Phys. Lett. B 73 (1978) 105.
[46] M. Holder, et al., Phys. Lett. B 69 (1977) 377.
[47] A. Bazarko, et al., Z. Phys. C 65 (1995) 189.
[48] P. Vilain, et al., Eur. Phys. J. C 11 (1999) 19.
[49] D. Mason, et al., Phys. Rev. Lett. 99 (2007) 192001.
[50] P. Astier, et al., Phys. Lett. B 486 (2000) 35.
[51] A. Kayis-Topasku, et al., Phys. Lett. B 527 (2002) 173.
[52] P. Astier, et al., Phys. Lett. B 526 (2002) 278.
[53] V.N. Gribov, L.N. Lipatov, Sov. J. Nucl. Phys. 15 (1972) 438.
[54] Y.L. Dokshitzer, et al., Sov. J. J. Exp. Theor. Phys. 46 (1977) 641.
[55] G. Altarelli, G. Parisi, Nuclear Phys. B 126 (1977) 248.
[56] J.G. de Groot, et al., Z. Phys. C 1 (1979) 143.
[57] B. Lampe, E. Reya, Phys. Rep. 332 (1990) 1.
[58] D. Geigerat, et al., Phys. Lett. B 245 (2002) 271.
[59] J. Dorenbosch, et al., Z. Phys. C 41 (1989) 567.
[60] Abramowicz, et al., Z. Phys. C 15 (1982) 19.
[61] J.V. Allaby, et al., Phys. Lett. B 231 (1989) 317.
[62] W.G. Seligman, et al., Phys. Rev. Lett. 79 (1997) 1213.
[63] G.P. Zeller, hep-ex/0110059, 2001.
[64] J.S. Ma, et al., Phys. Rev. D 73 (2006) 057302.
[65] K. Nakamura, et al., J. Phys. G 37 (2010) 075021.
[66] V. Lyubushkin, et al., Phys. Rev. D 81 (2010) 092005.
[67] V. Lyubushkin, et al., Eur. Phys. J. C 63 (2009) 355.
[68] A. Aguilar-Arevalo, et al., Phys. Rev. D 82 (2010) 092005.
[69] C. Mariani, et al., Phys. Rev. D 83 (2011) 054023.
[70] A. Aguilar-Arevalo, et al., Phys. Rev. Lett. 103 (2009) 081801.
[71] C.T. Kullenberg, et al., Phys. Lett. B 682 (2009) 177.
[72] S.L. Adler, Phys. Rev. B 135 (1964) 963.

[73] D. Rein, L.M. Sehgal, Nuclear Phys. B 223 (1983) 29.
[74] P. Astier, et al., Nuclear Phys. B 621 (2002) 3.
[75] D. Naumov, et al., Nuclear Phys. B 700 (2004) 51.
[76] Choukanov, et al., Nuclear Phys. B 700 (2006) 51.
[77] P. Astier, et al., Nuclear Phys. B 601 (2001) 3.
[78] N. Agafonovar, et al., Phys. Rev. Lett. 115 (2015) 121802.
[79] P. Astier, et al., Nuclear Phys. B 609 (2000) 371.
[80] C. Giusti, A. Meucci, Eprint 1110 (2011) 4005.
[81] J.I. Nieves, et al., Eprint 1110 (2011) 1200.
[82] M. Martini, et al., Phys. Rev. C 81 (2010) 045502.
[83] Drakoulakos, et al., Hep-Ex 05 (2004) 002.
[84] A.A. Aguilar-Arevalo, et al., Phys. Rev. D 82 (2010) 092005.
[85] R. Gandhi, et al., Astropart. Phys. 5 (1996) 81.
[86] S.L. Glashow, Phys. Rev. D 118 (1960) 316.
[87] E. Aslanides, et al., Astro-Ph 9907 (1999) 432.
[88] Achterberg, et al., Phys. Rev. D 75 (2007) 102001.
[89] De los Heros, et al., Nucl. Instrum. Methods A (2011) 630.
[90] I. Kravchenko, et al., Astropart. Phys. 5 (2003) 81.
[91] S.W. Barwick, et al., Phys. Rev. Lett. 96 (2006) 171101.
[92] L. Wolfenstein, Phys. Rev. D 17 (1978) 2369.
[93] S.P. Mikheyev, A.Yu. Smirnov, Neural Comput. 9 (1986) 17.
[94] D.S. Ayres, et al., NOVATDR, Fermilab-Design-01 (2007).
[95] D.Z. Freedman, Phys. Rev. D 9 (1974) 1389.
[96] W.J. Marciano, A.I. Sanda, Phys. Lett. B 67 (1977) 303.
[97] C. Amsler, et al., Nucl. Instrum. Methods 396 (1997) 115.
[98] H.T. Wong, J. Li, Hep-Ex 02 (2002) 01001.
[99] P.B. Pal, L. Wolfenstein, Phys. Rev. D 25 (1982) 766.
[100] S.A. Bludman, Phys. Rev. D 45 (1992) 4720.
[101] C. Giunti, et al., Phys. Rev. D 43 (1991) 164.
[102] A. Boyarsky, et al., Phys. Rev. Lett. 113 (2014) 251301.
[103] R. Ramond, et al., Phys. Rev. C 24 (1981) 1203.